

# We are IntechOpen, the world's leading publisher of Open Access books Built by scientists, for scientists

6,900

Open access books available

186,000

International authors and editors

200M

Downloads

Our authors are among the

154

Countries delivered to

TOP 1%

most cited scientists

12.2%

Contributors from top 500 universities



WEB OF SCIENCE™

Selection of our books indexed in the Book Citation Index  
in Web of Science™ Core Collection (BKCI)

Interested in publishing with us?  
Contact [book.department@intechopen.com](mailto:book.department@intechopen.com)

Numbers displayed above are based on latest data collected.  
For more information visit [www.intechopen.com](http://www.intechopen.com)



# Vortices on Sound Generation and Dissipation in Musical Flue Instruments

Shigeru Yoshikawa

## Abstract

Musical flue instruments such as the pipe organ and flute mainly consist of the acoustic pipe resonance and the jet impinging against the pipe edge. The edge tone is used to be considered as the energy source coupling to the pipe resonance. However, jet-drive models describing the complex jet/pipe interaction were proposed in the late 1960s. Such models were more developed and then improved to the discrete-vortex model and vortex-layer model by introducing fluid-dynamical viewpoint, particularly vortex sound theory on acoustic energy generation and dissipation. Generally, the discrete-vortex model is well applied to thick jets, while the jet-drive model and the vortex-layer model are valid to thin jets used in most flue instruments. The acoustically induced vortex (acoustic vortex) is observed near the amplitude saturation with the aid of flow visualization and is regarded as the final sound dissipation agent. On the other hand, vortex layers consisting of very small vortices along both sides of the jet are visualized by the phase-locked PIV and considered to generate the acceleration unbalance between both vortex layers that induces the jet wavy motion coupled with the pipe resonance. Vortices from the jet visualized by direct numerical simulations are briefly discussed.

**Keywords:** edge tone, pipe tone, jet wave, jet-drive model, discrete-vortex model, vortex-layer model, vortex sound theory, flow visualization, acoustically induced vortex, PIV, direct numerical simulation

## 1. Introduction

Musical wind instruments have a mechanism converting the direct energy of the fluid flow into the alternative energy of the sound. Such a system is called the self-sustained oscillation system. The fluid flow that drives the instruments may be regarded as the aerodynamical sound source or aeroacoustical source. Wind instruments are a very extensive subject of research over the vibration theory, acoustics, and fluid dynamics. The interaction between the resonance of the instrument [called generically *flue instruments* such as an organ pipe, flute, and recorder in this chapter (see **Figure 1**)] and the jet as the aeroacoustical source will be adequately described in this chapter.

Fluid flow brings about vortices and then generates the sound as well. However, one of the essential characteristics of wind instruments is the resonance, which is an acoustic mechanism amplifying very small perturbations to periodic disturbances

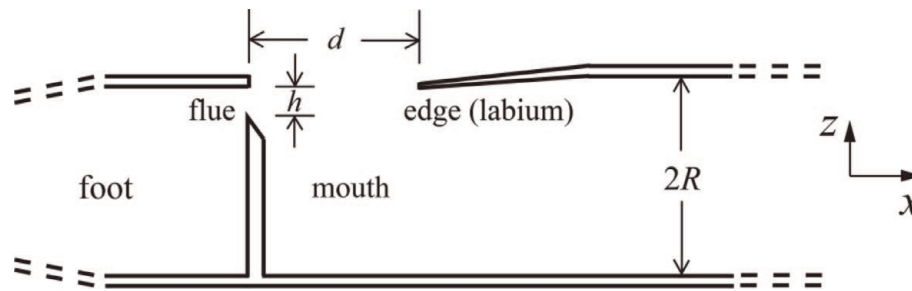


**Figure 1.**

An organ flue pipe as a typical example of the musical flue instruments and its important parameters.  $d$ , the flue-to-edge distance (or cutup, jet length);  $h$ , the jet thickness (or height of the flue exit);  $R$ , the pipe inner radius. The origin of the coordinate system is located at the center of the flue exit surface.

with large amplitudes. Any synchronization is then required, and it is realized by the suitable *phase relation* between the flow (or the jet) driving wind (or flue) instruments and the acoustic wave propagating in the instruments. For example, in the case of flue instruments, if the air flow enters into the pipe at the instant when the acoustic pressure near the edge takes a relatively large positive value, acoustic power (given by the product of the alternating volume flow and the acoustic pressure) becomes positive, and the sound is sustained.

However, a big dissatisfaction to the above viewpoint is the assumption of the existence of the sound at the starting point. Therefore, exactly saying, acoustical theory above is not sound generation theory but sound *regeneration* theory. The viewpoint of positive feedback between the jet and the pipe and the time-domain formulation based on the pipe reflection function [1] are both sound regeneration theory [2]. Musical instrument acoustics has treated such regeneration theories and phenomena as chief objects of research. This is because the resonance is acoustically essential, and we may consider that the resonance controls fluid movement as the energy source. It will be open to the charge of being imperfect combustion that sound existence is presupposed at the starting point when we try to answer how flue instruments produce their sounds.

Then, if we introduce a thesis, “the vortex itself is the true sound source,” of the vortex sound theory [3] to flue instruments, is the problem solved? Flue instruments do not seem to be such an obedient subject. Certainly, the vortex sound theory is satisfactorily valid to the edge tone, where the jet-edge system has no pipe that gives the resonance or the acoustic feedback; instead the fluid-dynamical feedback between the edge and the flue (flow issuing slit) is a main mechanism of sound generation.

Moreover, there are a few non-negligible differences other than the acoustic resonance between the edge tone and the pipe tone (or flue tone). First is the amplitude magnitude when the jet oscillates against the edge. The oscillation amplitude of the edge-tone jet is as small as two to three times the jet thickness. On the other hand, the pipe-tone jet in an organ pipe often exceeds 10 times the jet thickness. The edge in an organ pipe (or flue instruments) is just a partition wall which separates the inside from the outside of the pipe. It may be said that the direct jet-edge interaction time is quite short compared with a tonal period in flue instruments. Large vortices *visible* behind the pipe edge are, so to speak, odds and ends of the jet driving the pipe. We should pay more attention toward *invisible* (for our naked eyes) vortices carried along the jet to the edge.

Second is the difference in the jet-edge configuration. The configuration is usually symmetrical in the edge tone. In other words, the jet center surface corresponds to the edge tip. Alternate small vortices continuously appear above and beneath the edge. On the other hand, the edge is usually displaced upward in organ

pipes (see **Figure 1**). The flute may have such asymmetry depending on the player. This jet-edge divergence is called the *offset*, which is one of important parameters to adjust the tone color of flue instruments.

Also, we should relevantly notice largely different flow-acoustic interactions involved in various vortex-related sound generations. A thin jet and a sharp edge are used for the edge tone [4–6]. A thick (or semi-infinite) jet usually drives a wall-mounted cavity to produce its resonance called the cavity tone [7–9]. A thin jet drives a sharp edge (called the labium) of the resonant pipe to produce an organ pipe tone [1, 2, 10, 11]. A thin jet drives a thick edge with an angle of about  $60^\circ$  in the flute [1]. A thin jet issuing from a flue with the chamfer drives a sharp edge in the recorder [12, 13]. In addition, jet velocity widely extends from a few meters per second to about 50 m/s for these tone productions. Flow condition is laminar or turbulent. The Strouhal number  $St = fd/U_0$  ( $f$  the sounding frequency;  $d$  the flue-to-edge distance; and  $U_0$  the jet velocity at the flue exit) extends from about 0.05 to 5. Generally, a thin edge tends to enhance higher harmonics. As  $St$  has higher values, the jet flow, which drives the resonant pipe, tends to break down into *discrete vortices* [10, 14].

Although the vortex is essential in flow-excited sound generation, it may operate as an important source of acoustic energy dissipation in various flow-acoustic interactions [3, 15–17]. In the context of musical instruments, the *acoustically induced vortex* shedding at the edge is a key damping mechanism to determine the final amplitude of the steady-state flue instrument tones [16, 17]. Hence, sound dissipation and generation in flow-acoustic interactions are widely dominated by the vortex shedding at the edge [3].

Howe [18] assumes that a compact vortex core with relatively large size appearing alternately just above and below the pipe edge is created by the interaction between the jet velocity vector  $\mathbf{U}$  and the cross-flow velocity (acoustic reciprocating velocity) vector  $\mathbf{u}$  at the mouth opening formed between the flue and the edge. This vortex core with the vorticity  $\boldsymbol{\omega} (= \nabla \times \mathbf{U})$  is then considered to drive the air column in the pipe. The sound excitation by this periodic vortex shedding at the edge is controlled by the product of the aeroacoustic source term  $\text{div}(\boldsymbol{\omega} \times \mathbf{U})$  and the potential function representing the irrotational cross-flow  $\mathbf{u}$  at the mouth.

This discrete-vortex model of Howe is successfully applied to analyze and evaluate both cavity-tone generation [9] and tone generation in flue instruments [10, 14] when the jet is thick and the condition  $d/h < 2$  ( $d$  the width of the mouth opening or the flue-to-edge distance and  $h$  the jet thickness) is satisfied. On the other hand, when the condition  $d/h > 2$  is satisfied for thin jets, a jet-drive model on the basis of the intrinsic jet instability [19, 20] is applied instead of the discrete-vortex model [21]. This jet-drive model has been developed in the field of acoustics [1, 2, 11, 20, 22–27].

Although the jet-drive model has been proven to be effective for an explanation of sound generation by the thin jet, there remain rooms for improvement in applying the vortex sound theory for another explanation of sound generation by the thin jet in flue instruments because small vortices may be produced along the boundaries by the mixing process between the jet flow and the surrounding still air. The boundary layer consisting of small vortices is called the *vortex layer*, which can act as the source of an accelerating force to oscillate the jet. Based on such a viewpoint, the vortex-layer model was proposed recently [28].

In Section 2, the jet-drive, discrete-vortex, and vortex-layer models are described. Acoustically induced vortices (simply, acoustic vortices) on sound dissipation are discussed with the aid of flow visualization in Section 3. The jet vortex layer on sound generation in an organ pipe is visualized by the particle image velocimetry (PIV), and the microstructure of the vortex layer is demonstrated in

Section 4, and some examples of jet vortices are also introduced from experiments and simulations. Conclusions are given in Section 5.

## 2. Models on sound generation in flue instruments

### 2.1 Jet-drive model

#### 2.1.1 Volume-flow drive vs. pressure (momentum) drive

Jet motion in an organ pipe model when the jet drive is operating at the steady state is depicted in **Figure 2**. The air jet smoked with incense sticks is observed by a stroboscope and recorded on a VTR (8-mm video cassette) as analog data [2]. The pipe length  $L$  is 500 mm, the flue-to-edge distance (cutup length)  $d$  10.2 mm, and the jet thickness  $h$  at the flue exit 2.2 mm [2, 17]. The blowing pressure is 200 Pa (the jet velocity at the flue exit is estimated from Bernoulli's law to be 18.3 m/s). The sounding frequency is 285 Hz. One period  $T$  of the jet motion is divided by 9 in **Figure 2**.

As shown in **Figure 2**, the jet oscillates up and down. It does not break into vortices but keeps a diaphragm-like shape in the jet-drive operation. Large vortex-like air observed above the edge will not take a part in the sound generation. It is a kind of odds and ends of the jet driving the pipe. Also, it should be noticed that the jet behaves like an amplifying wave as inferred from the first six frames [29].

When the jet enters the pipe passing through the mouth area between the flue exit and the edge, the jet provides the pipe with the acoustic volume flow  $q(t)$  that is roughly approximated by the product of jet velocity  $U_e$ , jet breadth  $b$ , and jet lateral displacement  $\xi_e(t)$  (these quantities are given at the edge):

$$q(t) \approx -U_e b \xi_e(t), \quad (1)$$

where  $t$  is the time. The minus sign is needed from the definition that  $\xi_e(t)$  is positive outward and  $q(t)$  is positive inward. Eq. (1) defines the volume-flow model that was first proposed by Helmholtz [30] and utilized by many researchers afterwards for small amplitudes of jet oscillation [1, 2, 10–13, 20, 21, 24–27]. At the same time, the jet provides the pipe with the acoustic pressure produced by the momentum exchange with still air in the pipe:

$$p(t) = \rho U_e^2 (S_j/S_p), S_j \approx b \xi_e(t), \quad (2)$$

where  $\rho$  is the air density,  $S_j$  the temporally varying cross section of the jet entering the pipe from the edge, and  $S_p$  the pipe cross section. Eq. (2) defines the jet pressure of the jet momentum model, which was first proposed by Rayleigh [19] and utilized by many researchers afterwards [1, 2, 10–13, 21–27]. Opposing Helmholtz, Rayleigh insisted that the momentum drive should be effective. This is based on that the pipe is open and the acoustic power is produced by the product of the acoustic particle velocity near the pipe edge and the driving pressure given by the jet. However, the acoustic pressure considerably remains near the pipe edge due to the end correction. As a result, the volume-flow drive of Helmholtz is usually predominant except for the jet drive with very high blowing pressures [1, 2, 10, 21, 24, 25, 27].

The jet-drive model based on the volume-flow drive and the pressure drive was first formulated by Elder [24] by deriving the so-called jet momentum equation and then simplified by Fletcher [25]. They assumed a small control volume with length

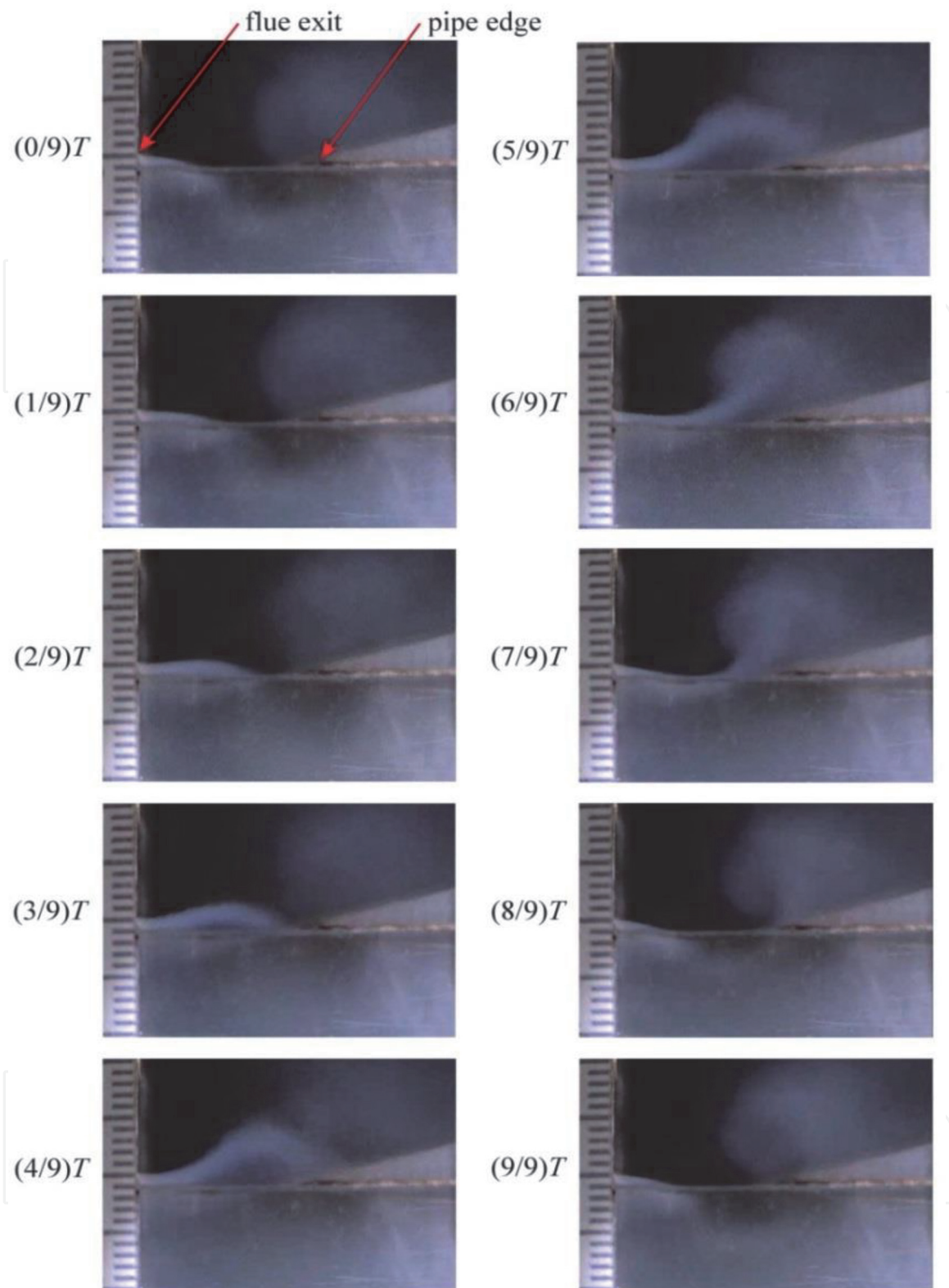


**Figure 2.**  
*Stroboscopically visualized jet oscillation at the steady state caused by the jet drive of an organ pipe model made with the acrylic resin.*

$\Delta x$  below the pipe edge. The turbulent mixing takes place over this control volume. The loss of jet momentum there will result in the simple pressure rise at the inner plane of the control volume. The net force on the control volume due to this pressure rise can then be equated to the rate at which jet momentum changes in the control volume [24]. In other words, just as “the momentum difference equals to the force impulse,” the momentum-flow-rate difference gives the force that accelerates the mass of the control volume.

It should be noticed that there is an appreciable phase difference between the volume-flow drive and the pressure drive. This phase difference is not well understood from Eqs. (1) and (2). The acoustic impedance or admittance should be introduced to connect these equations. According to Fletcher [1], this phase difference  $\phi$ , which gives the phase lag of the pressure drive, is given by:

$$\phi = -\tan^{-1}(U_e/\omega\Delta L), \quad (3)$$

where  $\omega$  is the angular frequency and  $\Delta L$  the effective mouth length including the open end correction. Since  $\omega\Delta L > U_e$  in usual cases,  $\phi$  is quite small. However, as mentioned above,  $\phi$  becomes appreciably large when the high blowing pressure is applied. See [1, 2, 10, 24–27] for more discussion on the complex jet/pipe interaction in flue instruments and on the conditions of the phase and amplitude for sound regeneration.

### 2.1.2 Jet wave and its amplification

Each frame in **Figure 2** does not show the path of air particle, but corresponds to the snapshot of the position of air particle at a given instant. Therefore, each frame indicates the *streak line* in the fluid-dynamical sense. On the other hand, the jet particle pass (*pass line*) may be determined as soon as the jet issues from the flue to the acoustic field in the mouth [26]. If the jet pass line can be determined, the jet deflection shape as the streak line may be estimated by considering the transit time of the particle issued from the flue exit [2, 26]. However, in the field of musical acoustics, the image visualizing the jet oscillation at the steady state in **Figure 2** has been called the *jet wave*, which seems to give the transverse displacement (in  $z$  direction) of the jet (cf. **Figure 1**).

It is assumed that the jet displacement may be expressed as a superposition of a progressive wave due to the jet instability [19, 20] and a spatially uniform oscillation induced by acoustic velocity  $u$  through the mouth as follows [1, 31]:

$$\xi(x, t) = (u/\omega) \{ -\cosh(\mu x) \sin[\omega(t - x/U_{ph})] + \sin(\omega t) \}, \quad (4)$$

where  $\xi(x, t)$  denotes the transverse displacement of the jet at distance  $x$  from the flue exit. Also,  $\mu$  and  $U_{ph}$  denote the amplification factor and phase speed of the instability wave, respectively, while  $u$  is the transverse acoustic velocity of the mouth field. The jet displacement  $\xi_e(t)$  in Eqs. (1) and (2) is given by  $\xi(x = d, t)$ . It should be noted that  $\xi(x)$  and  $u$  are positive in the external (positive  $z$ ) direction. Both  $\mu$  and  $U_{ph}$  are functions of  $x$  in a rigorous sense. Also, it is important that  $\omega$  in Eq. (4) corresponds to the fundamental of a sound generated. When very high blowing pressures are applied, the effect of the second harmonic is significant and the jet strikes the edge downward twice a period. Such an effect is excluded in Eq. (4). Also, an important parameter, jet thickness  $h$  is not included in Eq. (4), and a thin jet ( $d/h > 2$ ) is assumed. Although Eq. (4) lacks its physical basis and experimental confirmation, it is a simple and practical representation of the jet deflection that describes our current knowledge. So, we postulate in this chapter that Eq. (4) is valid in the acoustical sense.

The envelope of positive and negative peak displacements is yielded from Eq. (4) as follows:

$$\xi_{env}(x) = \pm(u/\omega) [\cosh^2(\mu x) - 2 \cosh(\mu x) \cos(\omega x/U_{ph}) + 1]^{1/2}. \quad (5)$$

Since the  $\cos(\omega x/U_{ph})$  dependence diminishes as  $\mu x$  becomes larger than one, it may be reasonable to approximate the second term in square bracket of Eq. (5) as  $2 \cosh(\mu x)$ . We then obtain the following simple expression [29]:

$$\xi_{env}(x) \approx \pm (u/\omega)[\cosh(\mu x) - 1]. \quad (6)$$

**Figure 3** shows the transverse displacements of the jet oscillation and their approximated envelopes (indicated by the broken line) at the steady state which are calculated by Eqs. (4) and (6), respectively. The following parameter values are supposed: the mouth-field strength  $u/\omega = 1$  (mm),  $\mu = 0.20$  ( $\text{mm}^{-1}$ ),  $\omega = 2\pi \cdot 133$  (rad/s),  $k = \omega/U_{ph} = 0.073 + 0.01x$  ( $\text{mm}^{-1}$ ),  $U_{ph}(x = 0) = U_0 = 11.5$  (m/s). The slowdown of  $U_{ph}$  is assumed so that  $k$  may be proportional to  $x$  in order to make calculation easier. For more detailed information, refer to [29].

The jet displacements from  $t = (3/10)T$  to  $t = (8/10)T$  in **Figure 3** almost correspond to those from  $t = (2/9)T$  to  $t = (7/9)T$  in **Figure 2**, though the flue-to-edge distance  $d$  is not the same ( $d = 10.2$  mm in **Figure 2** and  $d = 15.8$  mm in **Figure 3**). This good correspondence proves the effectiveness of the displacement model based on Eq. (4).

It is possible to directly estimate  $\mu$  from Eq. (4) by applying it to the experimental data. However, such an approach needs exact information about  $U_{ph}$  and a time reference. Another much simpler method to estimate  $\mu$  is to apply Eq. (6) to the experimental data. The result is shown in **Figure 4** for the first mode of an organ pipe model with  $L = 50.0$  cm and  $d = 10.2$  mm (cf. **Figure 2**) [29]. If a high-speed digital video camera is used instead of a stroboscope, the frames showing the jet waves such as given in **Figure 2** are digitally memorized, and then the digital superposition of these data yields a direct superposition of jet waves.

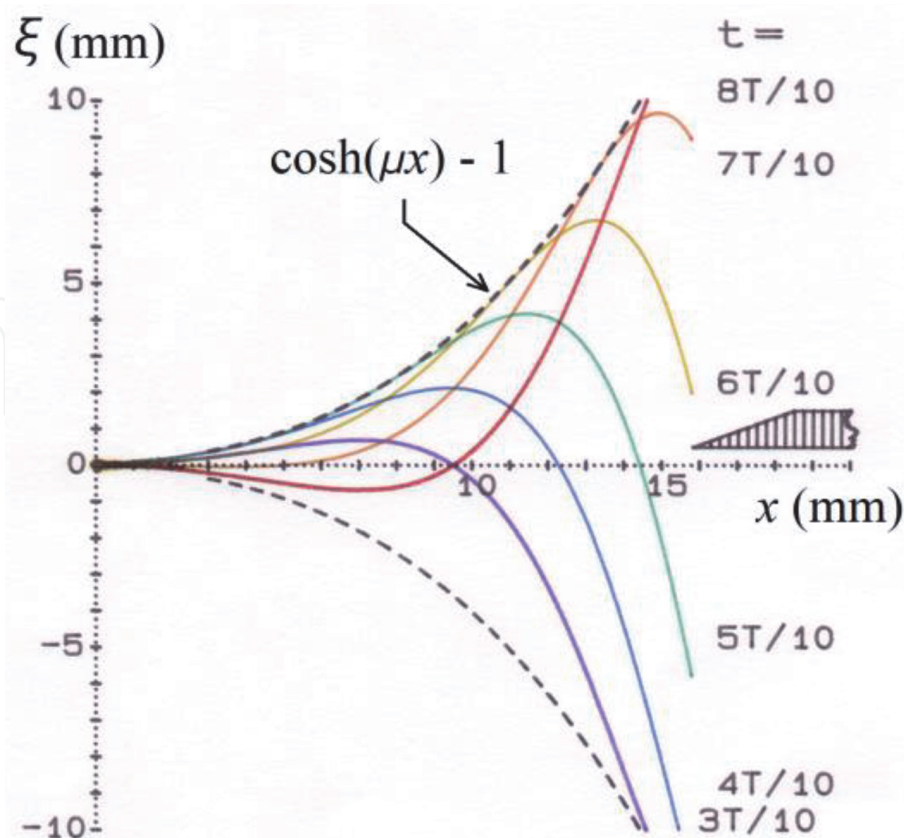


**Figure 3.**  
 The jet displacements calculated at the instants from  $3 T/10$  to  $8 T/10$  and their approximated envelope (the negative envelope is also indicated).

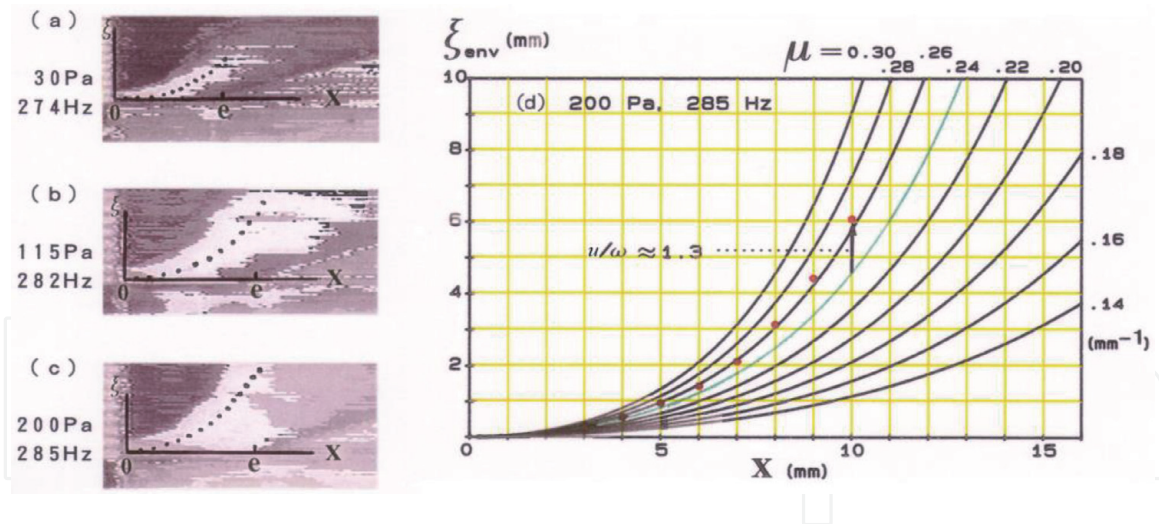


**Figure 4.**

Digitally superposed jet waves for different blowing pressures (a)–(c) and an illustration of how to derive the amplification factor  $\mu$  and the mouth-field strength  $u/\omega$  (d). The envelope of jet center-planes is estimated by the red dotted line that best fits to the green template curve with  $\mu = 0.24 \text{ mm}^{-1}$  and  $u/\omega = 1$ . The amplitude ratio of the dotted line to the green line determines  $u/\omega = 1.3 \text{ mm}$ .

Digitally superposed jet waves are shown in frames (a), (b), and (c) for different blowing pressures in **Figure 4**, where the  $x$  axis is drawn straightforwardly from the flue center labeled as “0,” and label “e” indicates the edge position. Frame (d) on the right of **Figure 4** illustrates how the jet envelope function is derived. The envelope of jet center-planes (indicated by dotted lines in **Figure 4**) is almost parallel to the outer fringe of the superposed jet waves as long as significant spreading of the jet can be neglected by using thin smokes for visualization. More details on the estimation of  $\mu$  from flow visualization are given in [29].

In **Figure 4(d)** the estimated envelope is shown by dots on a template, that is, curves of jet envelope function  $\cosh(\mu x) - 1$  for various  $\mu$  values assuming that  $u/\omega = 1$ . **Figure 4(d)** suggests a close fit of the dotted line to an envelope curve with  $\mu = 0.24 \text{ mm}^{-1}$  when the magnitude ratio of the dotted line to that curve is about 1.3. This ratio determines  $u/\omega = 1.3 \text{ mm}$  from Eq. (6).

Flow visualization suggests the following general trends from the result summarized in **Figure 5** on a particular experimental model of the organ pipe:

1. The amplification factor  $\mu$  tends to decrease and saturate to a given value as the oscillation of each mode shifts toward higher blowing velocities, although the data on the second mode are not sufficient.
2. The averaged amplification factor is roughly estimated as  $0.24 \text{ mm}^{-1}$ .
3. The mouth-field strength  $u/\omega$ , which means the displacement amplitude of the acoustic field at the mouth, tends to increase and saturate to a given value as the oscillation of each mode shifts toward higher blowing velocities.

It should be noted here that the estimate of  $\mu$  based on Eq. (6) tends to be a little larger (about 10%) than that based on Eq. (4). However, this estimation error is roughly equivalent to the resolution of the experimental data [29].

In order to confirm the validity of our digital superposition explained above,  $u/\omega$  was determined from measurements of the acoustic particle velocity  $u$  with a hot-wire anemometer (its sensing part is 1-mm long and  $5 \mu\text{m}$  in diameter) and of the sounding frequency  $\omega/2\pi$  (about 280 Hz in the first mode) with a microphone located inside the pipe. It is important to avoid exposing the hot-wire probe to the

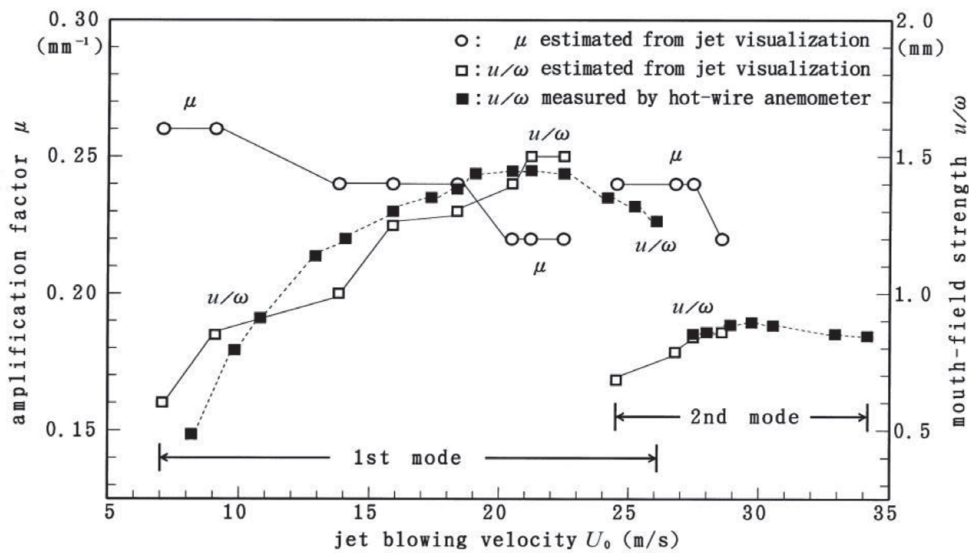


**Figure 5.** The amplification factor  $\mu$  and the mouth-field strength  $u/\omega$  of the organ pipe jet as functions of the jet velocity  $U_0$  at the flue exit [29]. The symbols  $\circ$  and  $\square$  indicate  $\mu$  and  $u/\omega$  estimated from the digital superposition based on the jet visualization, respectively. The symbol  $\blacksquare$  indicates  $u/\omega$  measured by a hot-wire anemometer and a microphone.

jet flow for the measurement of  $u$  because  $u \ll U_0$ . Therefore, after carrying out a preliminary experiment to select proper positions of the probe, the rms acoustic particle velocity  $u_{\text{rms}}$  was measured as the rms output voltage  $V_{\text{rms}}$  of the hot-wire anemometer ( $u = \sqrt{2}u_{\text{rms}}$ ) [29]. The result of  $u/\omega$  is indicated by the closed square in **Figure 5**.

Comparing the values of  $u/\omega$  measured using the hot-wire anemometer with those estimated from flow visualization, we may see a good agreement between them. This agreement implies that the method of deriving the envelope function of the jet wave is valid and sufficiently accurate. However, we had particular difficulty in obtaining a smooth jet-wave envelope near saturation, and the estimated data of  $\mu$  and  $u/\omega$  were lacking in **Figure 5**. This was due to other jet waves which were generated by the second harmonic and superposed upon the jet waves generated by the fundamental.

The origin of the jet-wave amplification is the jet instability. The applicability of the spatial and temporal theories on the jet instability [1, 32–34] to organ pipe jets can be discussed. If we assume a Poiseuille flow at the flue exit and a subsequent Bickley jet, the spatial theory [32, 33] seems to be relevant to organ pipe jets [29].

### 2.1.3 Jet-drive model for large jet displacements

The jet-drive model described above has supposed small displacements of the jet at the pipe edge. However, as demonstrated in **Figures 2–4**, the jet displacement is too large to apply Eqs. (1) and (2) to the sound generation in flue instruments in rigorous sense. According to Dequand et al. [21] and Verge et al. [27], a jet-drive model reasonable for large jet displacements is explained and roughly formulated below.

As understood from **Figures 2 and 3**, the passage time of the jet from one side to the other side of the edge seems to be very short compared to the oscillation period. In other words, the jet seems to be instantaneously switching from the inside to the outside of the pipe and vice versa. Then, the jet volume flow may be assumed to be split into two complementary antiphase monopole sources  $q_{\text{in}} [= |q| \exp(i\omega t)]$  and  $q_{\text{out}} (= -q_{\text{in}})$  whose temporal waveforms are rectangular pulses with the same

amplitude  $|q|$  [27]. These sources are supposed to be placed at a distance  $\epsilon$  from the edge tip at the lower and upper sides of the edge.

The acoustic pressure  $p_j(t)$  is derived from the potential difference across the mouth induced by two monopole sources [21, 27]:

$$p_j(t) = -\rho(\delta_j/bd)(dq/dt), \quad (7)$$

where  $\rho$  is the air density,  $b$  the jet (or mouth) breadth,  $d$  the flue-to-edge distance (or the mouth length), and  $\delta_j$  the effective distance between the two monopole sources. If  $\epsilon \ll d$ , we have from [27].

$$\delta_j/d \approx (4/\pi)\sqrt{2\epsilon/d}. \quad (8)$$

In the limit of thin jets ( $d/h \gg 1$ ), where  $h$  denotes the jet thickness at the flue exit,  $\epsilon = h_e$  (the jet thickness at the edge) is assumed [27].

The power generated by the source is calculated by assuming that the source is in phase with the acoustic volume flow  $q_m(t) = (d\xi_m/dt)db = udb$  through the mouth opening, where  $\xi_m$  denotes the particle displacement over the mouth opening [21]. This  $q_m$  is supposed to be a local two-dimensional incompressible flow. The above in-phase relation between the pressure source  $p_j$  and the acoustic volume flow  $q_m$  gives the condition for which the oscillation amplitude has a maximum as a function of the blowing pressure.

The time average over an oscillation period  $T$  of the power generated by the jet drive above is given as follows [21]:

$$\langle \Pi_{\text{jet}} \rangle = \langle p_j q_m \rangle \approx (8/\pi T)\rho\sqrt{2h_e/d}U_0 h_e b d |d\xi_m/dt|. \quad (9)$$

In addition to the thin jet assumption ( $d/h \gg 1$ ), we have to suppose that the jet does not break down into discrete vortices. This is only reasonable for the first hydrodynamic mode ( $S_t = fd/U_0 < 0.3$ ). The validity of Eq. (9) will be discussed in Section 3 after deriving the acoustic energy loss due to vortex shedding at the edge.

## 2.2 Discrete-vortex model

### 2.2.1 Discrete-vortex model based on the vortex shedding at the edge

On the basis of the two-dimensional theory, Howe [18] proposed a discrete-vortex model on sound generation in flute-like instruments. He assumed that a compact vortex core appearing alternately just above and beneath the edge was created by the interaction with the acoustic cross-flow velocity  $\mathbf{u}$  [ $d\xi_m/dt$  in Eq. (9) corresponds to one-dimensional ( $z$  direction) component] at the mouth opening (see **Figure 6**). That is, instead of the jet oscillation over the mouth explained in the previous section, a point vortex is produced at the edge. Then, this vortex core is assumed to drive the air column in the pipe. A discrete-vortex model for thick jets assumes that a discrete vortex is generated from the flow separation at the flue exit corner [9, 10, 21], while Howe [18] attached greater importance to the flow separation (vortex shedding) at an opposing sharp edge due to the acoustic cross-flow.

The sound excitation by the periodic vortex shedding at the edge is controlled by the product of the aeroacoustic source term  $\text{div}(\boldsymbol{\omega} \times \mathbf{v})$  and the potential function  $\phi(\mathbf{y})$  representing the irrotational cross-flow into and out of the mouth as expressed by the following integral [18]:

$$I(t) = \int \operatorname{div}(\boldsymbol{\omega} \times \boldsymbol{v})\phi(\boldsymbol{y})d^3\boldsymbol{y} = - \int (\boldsymbol{\omega} \times \boldsymbol{v}) \cdot \nabla\phi(\boldsymbol{y})d^3\boldsymbol{y}, \quad (10)$$

where the vorticity  $\boldsymbol{\omega}$  is defined as  $\operatorname{rot} \boldsymbol{v}$  and the velocity  $\boldsymbol{v}$  is the superposition of the jet mean flow velocity  $\boldsymbol{U}$  directing against the edge and the time-dependent cross-flow velocity  $\boldsymbol{u}$  that is specified by reciprocating potential flow through the mouth opening (see **Figure 6**). That is,  $\boldsymbol{v}$  is given by:

$$\boldsymbol{v} = \boldsymbol{U} + \boldsymbol{u}. \quad (11)$$

Also,  $\boldsymbol{y}$  denotes the source region (vortical field) of the pipe mouth over which the integral of Eq. (10) is performed. The specific form of  $\phi(\boldsymbol{y})$  is given as  $\phi_2^*(\boldsymbol{y})$  of Eq. (10.42) in [18].

According to [3], the power density supplied from the acoustic field to the vortical field around the edge is given by:

$$(1/2)(\partial/\partial t)(\rho v^2) = \rho(\boldsymbol{\omega} \times \boldsymbol{v}) \cdot \boldsymbol{u}. \quad (12)$$

Therefore, if  $(\boldsymbol{\omega} \times \boldsymbol{v}) \cdot \boldsymbol{u} > 0$ , it may be said that the energy of the acoustic field is absorbed by the vortical field. As a result, an *acoustically induced vortex* or *acoustic vortex* is generated [16, 17]. The generation of it satisfies the phase relation in which a clockwise-rotating vortex appears above the edge when  $\boldsymbol{u}$  directs into the pipe [see **Figure 12(b)** in Section 3.2.1]. This phase relation is contrary to that illustrated in **Figure 6**. A discrete vortex of Howe's type has not been observed in sound generation of flue instruments where jets are used in normal conditions [16, 17, 20–27, 29].

Howe [3, 35] then proposed the *acoustic dissipation formula*:

$$\Pi_D(t) \approx \iiint \rho(\boldsymbol{\omega} \times \boldsymbol{v}) \cdot \boldsymbol{u}dV, \boldsymbol{v} \approx \boldsymbol{U}. \quad (13)$$

This equation determines the rate of dissipation of acoustic energy, where  $\nabla\phi$  in Eq. (10) is now simply denoted by  $\boldsymbol{u}$ . Also,  $V$  denotes a volume enclosing the vorticity formed in the flow field. This  $\Pi_D$  of Eq. (13) can be negative in oscillation systems: If the phase of vorticity production enables a steady transfer of energy to the oscillation from a mean flow, the self-sustained oscillation can be maintained.

Hence, the *acoustic generation formula* may be proposed:

$$\Pi_G(t) \approx - \iiint \rho(\boldsymbol{\omega} \times \boldsymbol{U}) \cdot \boldsymbol{u}dV, \boldsymbol{\omega} = \operatorname{rot}\boldsymbol{U}, \quad (14)$$

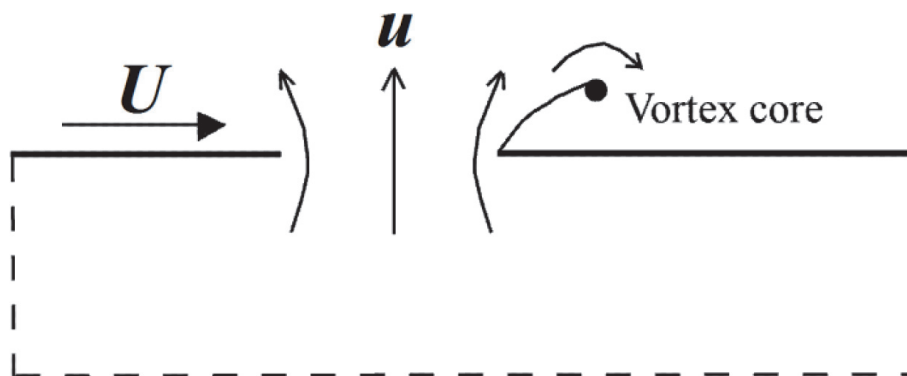


**Figure 6.** Conceptual sketch of a discrete-vortex model (the vortex shedding at the edge) for sound generation in flue instruments proposed by Howe [18].

where the vorticity  $\omega$  is simply given as  $\text{rot}U$ . If the time average  $\langle \Pi_G(t) \rangle$  is positive, the vorticity production from the jet flow supplies the acoustic power to the resonant pipe.

### 2.2.2 Discrete-vortex model based on the vortex shedding at the flue exit

When the jet is thick, the jet flow is not fully deflected into the resonant pipe. It is then difficult to apply the jet-drive model to thick jets. As the jet becomes thicker and thicker, the two shear layers at both sides of the jet tend to behave independently of each other. Meissner [9] described both shear layers in terms of discrete vortices (see **Figure 7**). He used the jet with  $h = 2.7$  mm (not so very thick). This jet excited a cavity resonator (its cross section: 40 mm  $\times$  28 mm; its depth: 12, 14, 16, 18, and 20 cm). The distance from the nozzle exit to the opposing orifice edge corresponding to the flue-to-edge distance  $d$  was set to be 8 mm ( $d/h = 2.96$ ). The orifice width was 28 mm, and the edge thickness 2 mm.

Meissner [9] found experimental results as follows: In stage I ( $5.9 \text{ m/s} < U_0 < 8.3 \text{ m/s}$ ), the frequency increased fast with the jet speed, and a frequency increment was proportional to the jet speed just as in the edge-tone generation [36, 37]. Similar phenomenon often appears at the very first stage in sound generation of flue instruments [1, 23]. In stage II ( $8.3 \text{ m/s} < U_0 < 16.1 \text{ m/s}$ ), an increase in the frequency was still observed, but a frequency growth was much smaller. The experimental results obtained for different cavity depths correlated reasonably well because data points corresponding to this stage approximately lay in one curve [9].

The cavity-tone generator shown in **Figure 7** can be considered as a simplified model of the ocarina. It is assumed that vorticity generation begins immediately after the jet issues from the nozzle exit due to flow separation. The vorticity of both shear layers is concentrated into line vortices traveling along straight lines with the convection velocity  $U_c$ . In the case of asymmetric vortex formation as shown in **Figure 7**, a configuration of vortices will be similar to that in the conventional Kármán vortex street. Thus,  $U_c$  may be approximated as that of an infinite street [9].

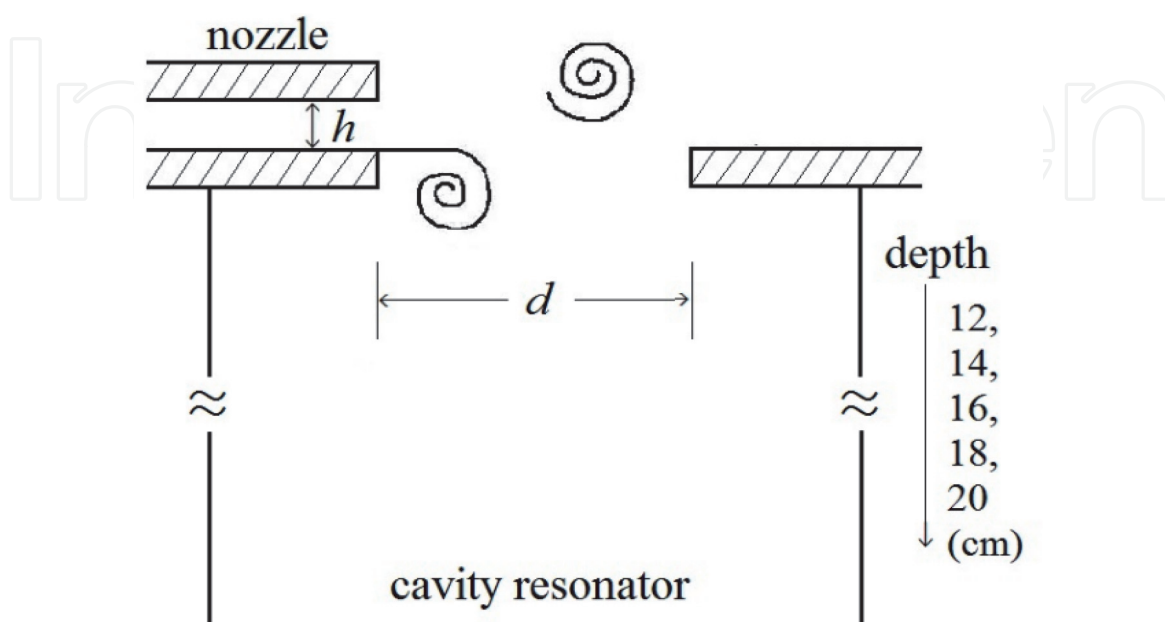


**Figure 7.** Vortex shedding in a cavity-tone generator [9], which can be considered as a simplified mechanical model of the ocarina.  $h = 2.7$  mm and  $d = 8$  mm.

$$U_c = (U_0/2) \tanh(\pi h/\lambda_v), \quad (15)$$

where  $\lambda_v$  is the distance between successive vortices in the lower and the upper line vortices and  $h$  is the distance between both lines which is equal to the jet thickness. It is also noted that the circulation  $\Gamma$  of the vortex increases linearly with the time according to  $\Gamma(t) = (1/2)U_0^2 t$ .

In the case of flue instruments with thick jets ( $d/h < 2$ ) [21], a new vortex is formed at the inner shear layer (on the resonant pipe side) each time the acoustic velocity  $d\xi_m/dt$  changes sign from directed toward the outside to directed toward the inside of the resonator (acoustic pressure in the resonator takes the minimum). A new vortex is formed at the outer shear layer half an oscillation period ( $T/2$ ) later (acoustic pressure in the resonator takes the maximum). In the steady state of oscillation, the circulation of the  $j$ th vortex ( $j = 1, 2, 3, \dots$ ) at the inner shear layer  $\Gamma_{in}^{(j)}$  and at the outer shear layer  $\Gamma_{out}^{(j)}$  can be written as [21].

$$\Gamma_{in}^{(j)}(t) = (1/2)U_0^2[t - (j - 1)T] \text{ for } (j - 1)T \leq t \leq jT, \quad (16)$$

$$\Gamma_{in}^{(j)}(t) = (1/2)U_0^2 T \text{ for } t > jT, \quad (17)$$

$$\Gamma_{out}^{(j)}(t) = -(1/2)U_0^2[t - (2j - 1)(T/2)], \quad (18)$$

for  $(2j - 1)(T/2) \leq t \leq (2j + 1)(T/2)$

$$\Gamma_{out}^{(j)}(t) = -(1/2)U_0^2 T \text{ for } t > (2j + 1)(T/2). \quad (19)$$

The acoustic power generated by the vortices is calculated by Eq. (14). The average of it over the oscillation period  $T$  is as follows:

$$\langle \Pi_{\text{vortex}} \rangle = -(1/T) \int_0^T \int_{V_s} \rho(\boldsymbol{\omega} \times \mathbf{U}) \cdot \mathbf{u} dV dt, \quad (20)$$

where the volume integration is taken over the source region of volume  $V_s$ . The vorticity field  $\boldsymbol{\omega} = \text{rot}\mathbf{U}$  takes into account the contribution of each vortex at the shear layers [21]:

$$\boldsymbol{\omega}(\mathbf{x}, y, t) = \sum_j \left[ \Gamma_{in}^{(j)}(t) \delta(\mathbf{x} - \mathbf{x}_{in}^{(j)}(t)) + \Gamma_{out}^{(j)}(t) \delta(\mathbf{x} - \mathbf{x}_{out}^{(j)}(t)) \right], \quad (21)$$

where  $\mathbf{x}$  defines a two-dimensional (2-D) point  $(x, y)$ ,  $\mathbf{x}_{in}^{(j)}(t)$  the position of the  $j$ th vortex at the inner shear layer, and  $\mathbf{x}_{out}^{(j)}(t)$  the position of the  $j$ th vortex at the outer shear layer.

It is first necessary to know the position and the circulation of vortices in order to calculate  $\langle \Pi_{\text{vortex}} \rangle$  from Eqs. (20) and (21). It was done by time-domain simulations in [38]. For the sake of paper space, see the details described in [38].

## 2.3 Flow visualization and some discussion

### 2.3.1 Jet-wave drive vs. discrete-vortex drive

Dequand et al. [21] visualized the steady-state periodic flow in the mouth of the resonator by applying a standard Schlieren technique. They used three types of flute-like mouth configuration with a common edge of  $60^\circ$ , a common sharp edged

flue exit, a common flue-to-edge distance  $d = 24$  mm, and different flue channel height (i.e., jet thickness)  $h = 4, 14,$  and  $30$  mm ( $d/h = 6, 1.7,$  and  $0.8$ ). The pipe length  $L$  was  $552$  mm. The initial jet velocity  $U_0$  had, respectively,  $16.3, 14,$  and  $14.5$  m/s ( $S_t = 0.19, 0.22,$  and  $0.22$ ). **Figure 8** summarizes their result by rough illustration, though the flow inside the pipe is not so clear in [21].

Frames in the left column [(a), (c), and (e)] show flow conditions at the phase of  $u = 0$  (the instant from the positive to the negative), while frames in the right column [(b), (d), and (f)] show flow conditions at the next phase of  $u = 0$  (the instant from the negative to the positive). Note that the positive  $u$  indicates the upward (outward) acoustic velocity here, but it indicates the downward (inward) acoustic velocity in [21]. Also, the flow visualization of each case is shown by eight frames consisting of one oscillation period [21].

The jet-wave drive illustrated in **Figure 8(a)** reveals that the jet enters into the pipe at the instant when the acoustic pressure  $p(t)$  is maximum because the phase

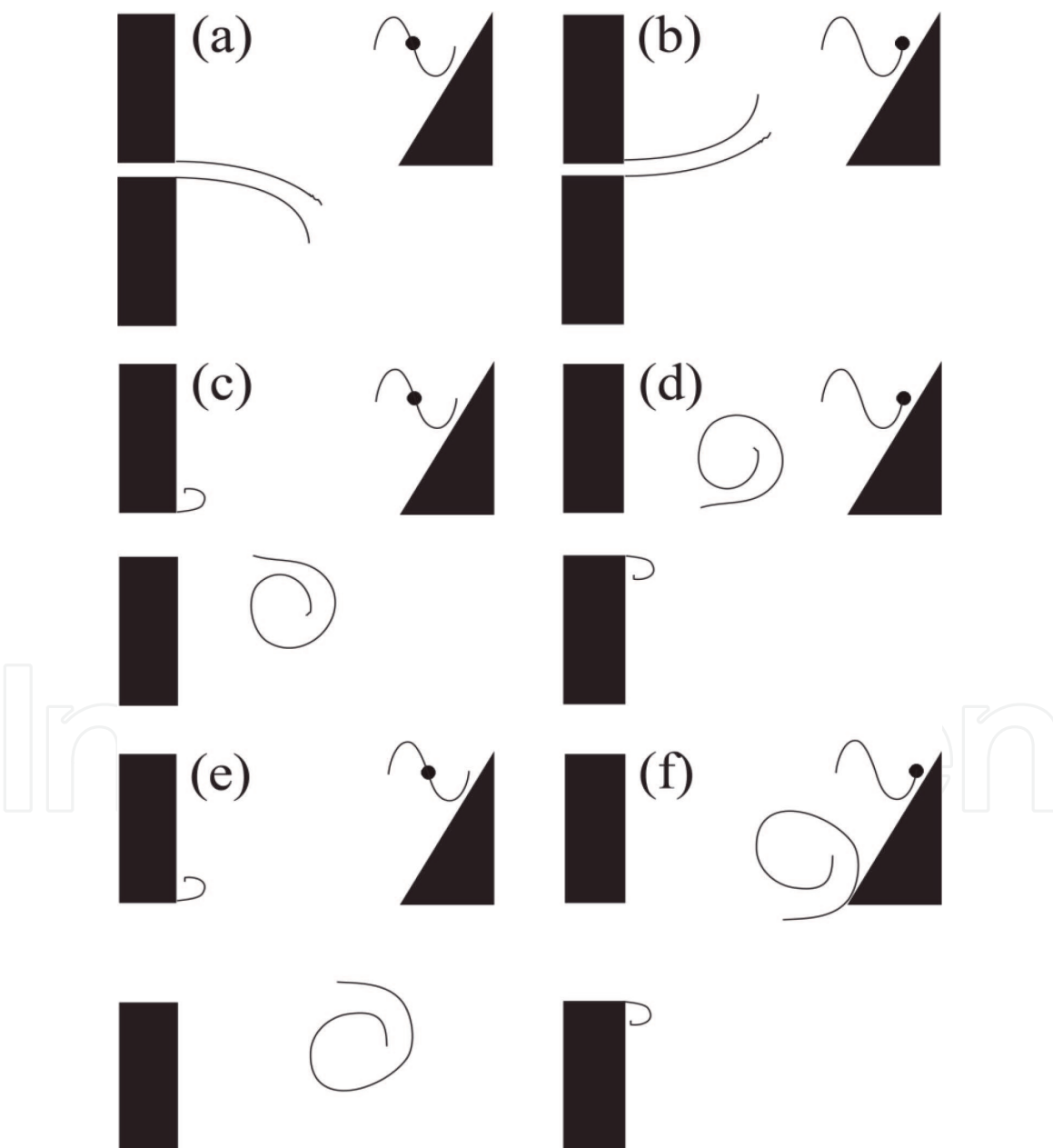


**Figure 8.** Illustrations of flow visualization by Dequand et al. [21]. Top two (a) and (b) have  $h = 4$  mm, middle two (c), and (d)  $h = 14$  mm, and bottom two (e) and (f)  $h = 30$  mm. The sinusoidal wave inserted in each frame depicts the acoustic velocity  $u$  in the mouth, and the dot gives its instantaneous phase. Note that  $u$  is positive upward (outward) here, but  $u$  is positive downward (inward) in [21].

of  $p(t)$  is delayed from  $u(t)$  by  $90^\circ$  at the resonance. Therefore, the positive acoustic power  $\langle p(t) \cdot q(t) \rangle$  is generated, where  $q(t)$  denotes the acoustic volume flow into the pipe [see Eq. (1)]. The positive acoustic power is also generated at the instant given in **Figure 8(b)**. As the result, the volume-flow drive in the jet-drive model is satisfied very well.

The discrete-vortex drive illustrated in **Figure 8(e)** indicates that the upper vortex is just created at the upper flue exit corner and the lower vortex reaches to the pipe edge in a fully developed shape. Also, **Figure 8(f)** indicates that the lower vortex is just created at the lower flue exit corner and the upper vortex is reached to the pipe edge in a fully developed shape. As a result, the positive acoustic power given by Eq. (20) or Eq. (14) is generated [see **Figure 9(b)** below].

Two illustrations of **Figure 8(c)** and **(d)** correspond to a boundary condition between the jet-wave drive and the discrete-vortex drive. Then, the lower and upper large vortices are located halfway between the flue exit and the edge. This is probably due to an opposing effect between both drives.

**Figure 9** summarizes the phase relation between the physical quantities involved in the jet-wave drive (a) and the discrete-vortex drive (b). The red dot on the sinusoidal curve of  $u$  corresponds to the phase of  $u$  in **Figure 8**. The time scale is converted to the integer by  $12(t/T)$ . The magnitude of physical quantities is arbitrary. The jet-wave drive indicates the antiphase relation between the jet displacement  $\xi_e(t)$  at the edge and the acoustic pressure  $p(t)$  in the resonant pipe. This result endorses the acoustic power generation in good manner (note that  $u$  and  $\xi_e$  are defined positive upward).

In the discrete-vortex drive, the horizontal arrow connects the vortex creation at the flue exit and the vortex arrival at the edge as shown in **Figure 9(b)**. Since the upper vortex rotates anticlockwise, the vector direction of  $\omega \times U$  in Eq. (20) is upward (positive  $z$  direction). During the passage of the upper vortex from the flue exit to the pipe edge, the acoustic cross-flow  $u$  in  $z$  direction has negative values. Hence,  $\langle \Pi_{\text{vortex}} \rangle$  of Eq. (20) takes a positive value during the latter half of an oscillation period. Similarly, the lower vortex produces positive  $\langle \Pi_{\text{vortex}} \rangle$  during the former half of an oscillation period. As a result, discrete vortices will create positive  $\langle \Pi_{\text{vortex}} \rangle$  in an oscillation period. In other words, the vortex configurations illustrated in **Figure 8(e)** and **(f)** may create the acoustic power for sound generation in flue pipes.

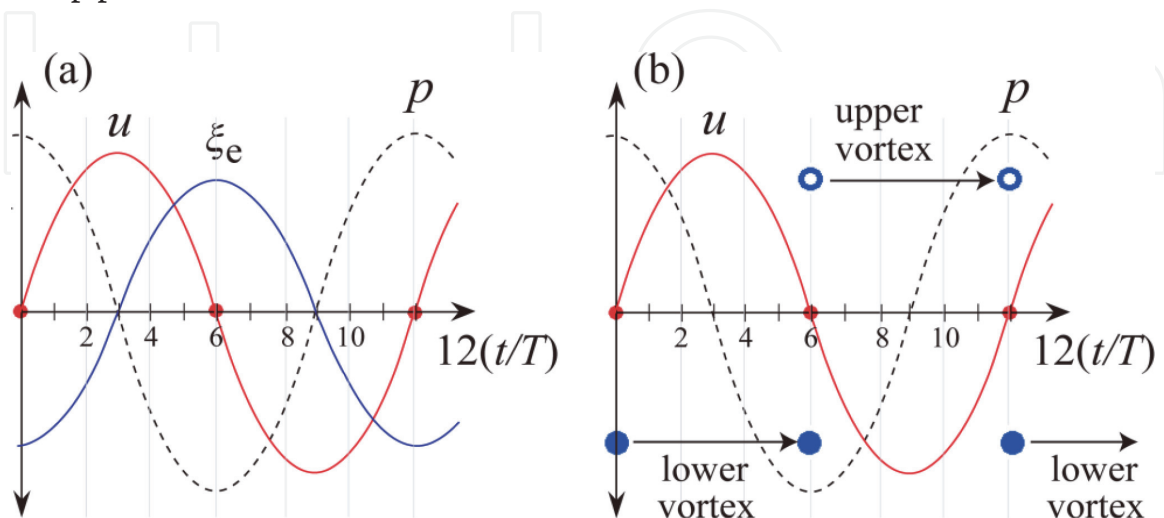


**Figure 9.** Phase relation between the physical quantities involved in the jet-wave drive (a) and the discrete-vortex drive (b). Their amplitudes are arbitrary. The red dot on the curve of  $u$  corresponds to the phase of  $u$  in **Figure 8**. The horizontal arrow in (b) connects the vortex creation at the flue exit and the vortex arrival at the pipe edge. Note that the positive direction of  $u$  and  $\xi_e$  is upward (outward) and the phase of  $p$  is delayed from  $u$  by  $90^\circ$  at the resonance.

### 2.3.2 Edge tone vs. pipe tone

The edge tone is a dipole source, whose acoustic pressure directly correlates with the vortex generation. That is, when the jet impinges the edge by moving from the downward to the upward, a vortex rotating clockwise is produced just below the edge, and another vortex rotating anticlockwise exists downstream above the edge. This configuration of the vortex pair generates the maximum acoustic pressure above the edge and the minimum acoustic pressure below the edge. When the jet impinges the edge by moving from the upward to the downward, a vortex rotating anticlockwise is produced just above the edge, and another vortex rotating clockwise exists downstream below the edge. This configuration of the vortex pair generates the maximum acoustic pressure below the edge and the minimum acoustic pressure above the edge [2, 39]. Although Eq. (14) cannot be applied to the edge tone since there is no acoustic feedback (i.e.,  $\mathbf{u} = 0$ ), the acceleration  $\boldsymbol{\omega} \times \mathbf{U}$  given by vortex rotation and jet velocity should be involved in the edge-tone generation. As a result, the edge tone satisfies:

$$\text{phase}[p_e(t)] - \text{phase}[\xi_e(t)] \approx \pm \pi/2, \quad (22)$$

where  $p_e(t)$  denotes the acoustic pressure below or above the edge. This phase relation is clearly different from that of the pipe tone shown in **Figure 9(a)**:

$$\text{phase}[p(t)] - \text{phase}[\xi_e(t)] \approx \pi. \quad (23)$$

The difference between the edge tone and the pipe tone is reflected in Eqs. (22) and (23) in good manner.

### 2.3.3 Feedback loop gain and time delay of the jet wave in the jet-drive model

Let us consider the feedback loop to find out the time delay of the jet wave which fulfills the phase condition for sound generation. As mentioned in Section 2.1.2, the jet particle pass may be determined as soon as the jet issues from the flue to the acoustic field in the mouth [26]. At that instant, the initial transverse displacement  $\xi_f(t)$  of the jet at the flue exit is supposed to be non-zero and related with the acoustic velocity  $u_f(t)$  at the flue exit as follows [38, 40]:

$$\xi_f(t)/h = u_f(t)/U_0, \quad (24)$$

where  $h$  and  $U_0$  are the jet thickness and jet velocity at the flue exit, respectively. The starting point of the feedback loop is  $u_f(t)$ , which creates  $\xi_f(t)$ . The jet displacement travels to the pipe edge as the jet wave, and we have at the edge [21].

$$\xi_e(t) = e^{ud} \xi_f(t - \tau_{jw}) = (h/U_0) e^{ud} u_f(t - \tau_{jw}), \quad (25)$$

which yields the acoustic pressure  $p_j(t)$  at the pipe entrance according to Eq. (7) in which  $q(t) \approx -U_e b \xi_e(t)$  from Eq. (1). Note that Eq. (25) largely simplifies Eq. (4) by considering the essential elements (spatial amplification and phase velocity) of the jet wave. The quantity  $\tau_{jw}$  denotes the time delay of the jet wave when it travels from the flue exit to the edge ( $\tau_{jw} = d/U_{ph}$ ).

The acoustic pressure  $p_j(t)$  drives the pipe and yields its resonance. As a result,  $u_f(t)$  at the starting point is fed back through the input admittance  $Y(\omega)$  of the pipe. The Fourier transform of  $p_j(t)$  is thus given by:

$$P_j(\omega) = (\rho h \delta_j / d)(i\omega) e^{\mu d} e^{-i\omega \tau_{jw}} U_f(\omega), \quad (26)$$

where  $U_f(\omega)$  is the Fourier transform of  $u_f(t)$  and  $U_e = U_0$  is assumed by neglecting the jet spreading for simplicity [41]. The feedback loop gain  $G(\omega)$  is thus defined as

$$G(\omega) = Y(\omega)[P_j(\omega)/U_f(\omega)]. \quad (27)$$

Hence, the phase condition for the self-sustained (feedback) oscillation is:

$$\text{phase}[G(\omega)] = \text{phase}[Y(\omega)] + \pi/2 - \omega \tau_{jw} = \pm 2m\pi \quad (28)$$

That is, the time delay  $\tau_{jw}$  of the jet wave must satisfy:

$$\begin{aligned} \omega \tau_{jw} &= \text{phase}[Y(\omega)] + \pi/2 + 2m\pi \\ &= \text{phase}[Y(\omega)] + \left(m + \frac{1}{4}\right)2\pi, \end{aligned} \quad (29)$$

where  $-2m\pi$  is abandoned because  $\omega \tau_{jw}$  is always positive and  $m$  ( $= 0, 1, 2, \dots$ ) denotes the hydrodynamic mode number. Usually, sound generation in flue pipes occurs for  $m = 0$ . Since  $\text{phase}[Y(\omega)] = \pi/2$  at the pipe resonance (see **Figure 9**), we finally have:

$$\tau_{jw} = \pi/\omega = T/2 \quad (30)$$

for the first mode  $m = 0$ . Therefore, it may be said that flue instruments are well excited when the time delay of the jet wave is around half an oscillation period. More detailed discussion is given in [38, 41]. Although the amplitude condition for sound generation can be calculated from Eq. (27), we do not have the space enough to do that.

#### 2.3.4 Time delay of vortex convection in the discrete-vortex model

According to **Figure 9(b)**, the upper and lower vortices created at the flue exit arrive at the pipe edge with a time delay of  $T/2$ , respectively. As explained in Section 2.3.1 the convection of these two vortices may create the acoustic power  $\langle \Pi_{\text{vortex}} \rangle$  defined by Eq. (20) for sound generation in flue pipes. Thus, the time delay of vortex convection  $\tau_{dv}$  in the discrete-vortex model is:

$$\tau_{dv} = d/U_c = T/2. \quad (31)$$

This Eq. (31) just corresponds to Eq. (30) in the jet-drive model. Therefore, both models provide the same dependence of the oscillation frequency on the jet velocity.

Although  $\tau_{dv}$  is easily derived from **Figure 9(b)**, it will be desirable to consider  $\tau_{dv}$  based on the phase balance such as in Eq. (29). The sound generation by the periodic pulse-like force (produced by each vortex arrival) at the edge will be maximum when the pulse is in phase with the maximum of acoustic velocity  $u$  at the edge. Since the vortex arrival occurs at the zero-crossing of  $u$  [see **Figure 9(b)**], the instant of the maximum  $u$  is given by  $\tau_{dv} - T/4$ , which should be balanced with the delay due to the input admittance  $Y(\omega)$  of the resonant pipe. Then, we have the following phase balance by allowing a time delay of  $m$  periods:

$$\tau_{dv} - \left(m + \frac{1}{4}\right)T = \text{phase}[Y(\omega)]/\omega. \quad (32)$$

This equation is the same as Eq. (29) when it is divided by  $\omega$ . A similar derivation of Eq. (32) is given in [38]. When  $m = 0$ , Eq. (31) is given from Eq. (32).

### 2.3.5 Aspect ratio $d/h$ of the jet

The aspect ratio  $d/h$  (jet length/jet thickness) is an essential parameter that discriminates the jet-drive model from the discrete-vortex model as indicated in **Figure 8** based on [21]. The value of  $d/h = 1.7$  set up in **Figure 8(c)** and **(d)** seems to be more favored by the discrete-vortex model. The critical aspect ratio that discriminates both models is  $d/h = 2.3$  in more rigorous sense [21, 38].

Dequand et al. [21] calculated  $|d\xi_m/dt|_{\max}/U_0$  as a function of  $d/h$  for both models, and experimental data on the flue exit with chamfered edges and the pipe edge with  $15^\circ$  were plotted on the calculated diagram (see Figure 12 in [21]). In very rough sense, the solution curve of the jet-drive model is proportional to  $(d/h)^{-1}$ , and that of the discrete-vortex model is proportional to  $(d/h)^{1/2}$ . The crossing of the two curves occurs near  $d/h = 2.3$ , and the experimental data approximately fit the discrete-vortex solution below this crossing and better fit the jet-drive solution above the crossing. Also, the experimental curve of data points indicates the maximum value at the crossing or the critical aspect ratio. It was experimentally confirmed on four kinds of the flue-edge geometry (see Figure 10 in [21]). Furthermore, Auvray et al. [38] extended similar calculation for different oscillation regimes ( $m = 0, 1; f = f_1, f_2$ ) (see Figure 8 in [38]). According to [38], the critical aspect ratio depends on the hydrodynamic jet mode  $m$ . For an eolian regime ( $m = 1, f = f_2$ ), the critical aspect ratio is much larger ( $d/h \cong 13$ ).

## 2.4 Vortex-layer model

Howe [18] and Dequand et al. [21] proposed the discrete-vortex model driven by thick jets ( $d/h < 2$ ) as explained in Section 2.2. However, there seems to be a room for the vortex even in the sound generation of flue instruments driven by thin jets that satisfy  $d/h > 2$ . Since an actual jet has a velocity profile as indicated by the broken line in **Figure 10(a)**, the vorticity can be formed along the boundary between the jet and the surrounding fluid. As the result, a layer (or sheet) of vorticity is organized along an immediate vicinity of the jet. The upper layer consists of the positive vorticity (the counterclockwise-rotating tiny vortices), and the lower layer consists of the negative vorticity (the clockwise-rotating tiny vortices). This physical picture depicted in **Figure 10(a)** may be called the vortex-layer model on the sound generation in musical flue instruments [2, 28].

It should be carefully noted that actual sound generation is three-dimensional (3-D) as inferred from the volume integral of Eq. (14), but our vortex-layer model illustrated in **Figure 10(a)** assumes the two-dimensionality (2-D). This 2-D assumption corresponds to the 2-D assumption of  $\mathbf{U}$  and  $\mathbf{u}$  that has been conventionally made in acoustical models. See Figures 10 and 11 in [28] on the 3-D nature of  $\mathbf{U}$  and  $\mathbf{u}$ . The PIV observation on a plane sheet by the laser (see Section 4.1 and **Figure 14**) is based on the 2-D assumption above.

Since  $\mathbf{u}$  is periodic, the time average  $\langle \Pi_G(t) \rangle$  should be null if  $\boldsymbol{\omega} \times \mathbf{U}$  is stationary in time as shown in **Figure 10(b)**. However, since the actual jet has any fluctuation, if  $\boldsymbol{\omega} \times \mathbf{U}$  has a component that changes temporarily in accordance with temporal change of  $\mathbf{u}$ , non-zero value of  $\langle \Pi_G(t) \rangle$  may be expected from the unbalance between

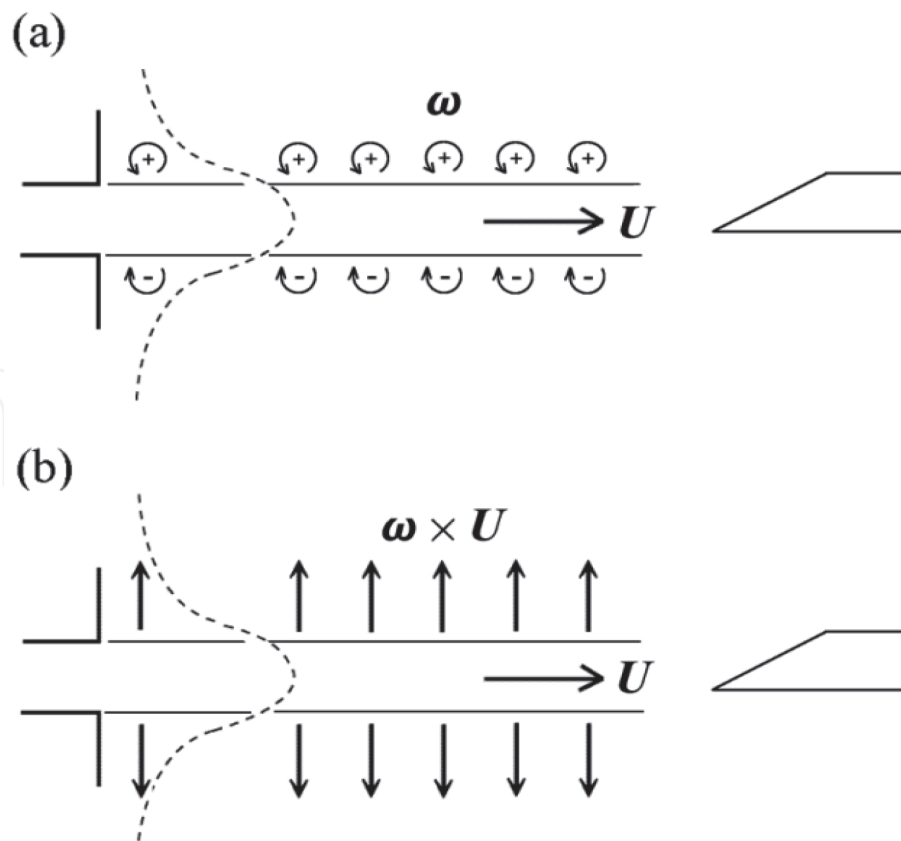


**Figure 10.** Conceptual sketch of the vortex-layer model on sound generation in flue instruments [2, 28]: (a) the vortex layers (consisting of tiny vortices) along both sides of the jet flow and (b) the generation and cancellation of the aeroacoustical source term  $\omega \times U$ . The dashed line depicts a lateral profile of the jet velocity  $U$ .

the upper and lower vortex layers. Hence, the sound generation in flue pipes may be yielded by the interaction between the jet vortex layer and the acoustic mouth flow. In this sense,  $\omega \times U$  and  $(\omega \times U) \cdot u$  may be called the *aeroacoustical source term* (with the same dimension as the acceleration) and the *acoustic generation term*, respectively.

Helmholtz [30] already suggested the importance of the jet vortex layer. His vortical surface (or stratum) that has a very unstable equilibrium acts as “an accelerating force with a periodically alternating direction” to reinforce the inward and outward velocity at the pipe entrance. Interestingly enough, this physical picture of Helmholtz is very similar to the jet vortex-layer model shown in **Figure 10** [2, 28]. It should be recognized that the volume-flow drive first proposed by Helmholtz [30] is based on his physical concept of the vortex layers formed along the jet flow.

### 3. Vortices on sound dissipation

#### 3.1 Sound dissipations in linear acoustics

Let us briefly discuss the mechanisms of sound dissipation (or absorption) in flue instruments because the self-sustained musical instruments must overcome the acoustic dissipations involved in them. At first let us consider within the field of linear acoustics and start from sound dissipation in free space.

##### 3.1.1 Classical absorption and molecular absorption in free space

In free space, the classical sources of dissipation are internal friction and heat conduction. Both phenomena tend to equalize the local variations of the particle

velocity and temperature accompanying the acoustic wave [42]. As a result, the acoustic energy is removed from the acoustic wave.

The equations on dissipation due to internal friction were derived by G. Stokes in 1845 and those on dissipation due to heat conduction by G. Kirchhoff in 1868. A plane sound wave is exponentially damped in the direction of propagation ( $x$  direction):  $e^{-\alpha x}$ . The coefficient  $\alpha_F$  of the dissipation due to internal friction is [42]

$$\alpha_F = (2\omega^2/3c^3)(\eta/\rho), \quad (33)$$

where  $c$  is the propagating sound velocity,  $\eta$  the dynamic viscosity, and  $\rho$  the air (or generally, gas) density. The coefficient  $\alpha_H$  due to heat conduction in gases is of the same order of magnitude as  $\alpha_F$  and is proportional to  $\omega^2$  [42]. The distance within which the sound level falls by 1 dB (an amplitude decrease of about 11%) due to classical absorption is very large in air (1-kHz wave gives 5 km; 10-kHz wave 50 m) [42]. Therefore, classical dissipation is almost negligibly weak.

The major source of strong dissipation in free space is molecular sound absorption. The translational and rotational energies of gas molecule are very quickly increased by a sudden impact, while the oscillatory energy builds up gradually at the expense of the translational and rotational energies [42]. The delay in reaching thermal equilibrium is called relaxation, and its time constant is called the relaxation time  $\tau_R$ . The source of molecular absorption in air is oscillatory relaxation of oxygen. The relaxation frequency (defined as  $1/2\pi\tau_R$ ) of pure oxygen is very low (about 10 Hz). However, the water vapor content of air greatly shortens the relaxation time and shifts the absorbing range into the audio frequencies (see Figure 3.7 in [42]). The acoustic dissipation in moist air is significantly greater than the classical absorption given by  $\alpha_F + \alpha_H$ .

### 3.1.2 Sound dissipation at the internal wall of a long pipe

Next let us consider the dissipation in the confined air instead of in free air. If a sound wave propagates in a long pipe where sound reflection can be neglected, it suffers additional losses because of internal friction and heat conduction in the boundary layer next to the wall. The acoustic particle velocity parallel to the pipe axis is zero at the internal wall surface because of friction (called no-slip condition). Its maximum value is not reached until the distance from the wall amounts to a quarter of viscosity wavelength  $\lambda_{vw}$  (see Figure 3.10 in [42]). This  $\lambda_{vw}$  characterizes the thickness of the wall boundary layer and is given by

$$\lambda_{vw} = 2\pi\delta = 2\pi\sqrt{2\eta/\omega\rho} \approx (1.4 \text{ cms}^{-1/2})/\sqrt{f}, \quad (34)$$

where  $\delta$  is the skin depth and the equation of the right-hand side is for the air with the kinematic viscosity  $\eta/\rho = 1.5 \times 10^{-5} \text{ m}^2 \text{ sec}^{-1}$  [42].

The losses occurring in the wall boundary layer due to viscous friction and heat conduction (the wall is considered as a surface with a constant temperature and the thermal change followed by the acoustic wave should be null at the wall surface) attenuate sound waves in pipes. A parameter to appropriately express the sound attenuation in a pipe is the ratio of the pipe radius  $R$  to the boundary layer thickness (or the skin depth)  $\delta$ . This ratio defines the quality factor  $Q$  or the inverse of the loss factor  $\zeta$  (generally,  $Q = \zeta^{-1} = R/\delta$ ). The values of  $Q$  for viscous friction and heat conduction are, respectively, given as [1, 43].

$$Q_v = (\omega\rho/2\eta)^{1/2}R, Q_t = (\omega\rho C_p/2\kappa)^{1/2}(\gamma - 1)^{-1}R, \quad (35)$$

where  $\eta$  denotes the viscosity of the air,  $C_p$  the specific heat at constant pressure,  $\kappa$  the thermal conductivity, and  $\gamma$  the ratio of specific heats. The ratio of thermal loss to viscous loss is given by  $Q_t^{-1}/Q_v^{-1} = 0.46$  for the air.

The attenuation constant  $\alpha_w$  of a round pipe is a function of the frequency  $f$  (in hertz) and the pipe radius  $R$  (in meters) [1, 42, 43]:

The attenuation constant  $\alpha$  in total is given by adding  $Q_{\text{rad}}^{-1}$  in Eq. (36):

$$\begin{aligned} \alpha_w &= (\omega/2c)(Q_v^{-1} + Q_t^{-1}) \approx 3.1 \times 10^{-5} (f^{1/2}/R) \text{ in m}^{-1} \\ &= 2.7 \times 10^{-4} (f^{1/2}/R) \text{ in dBm}^{-1}, \end{aligned} \quad (36)$$

where  $\alpha_w$  is approximately evaluated in  $\text{m}^{-1}$  and  $\text{dBm}^{-1}$ . The conversion is done by the relation  $\alpha_w(\text{in dBm}^{-1}) = 20 \log e \times \alpha_w(\text{m}^{-1}) = 8.68 \alpha_w(\text{m}^{-1})$  based on the exponential decay. For example, the modern flute with  $R \approx 10$  mm indicates  $\alpha_w \approx 0.85 \text{ dBm}^{-1}$  for  $f = 1000$  Hz. This attenuation is much larger than that occurs in free air, but still small enough. For example, tubes many meters long formerly were used on ships to transmit commands from the bridge to the engine room [42]. This large but still small enough magnitude of  $\alpha_w$  is the right reason why musical flue instruments and other wind instruments work out well. In order to suppress sound propagation in tubes (or in air conditioning systems) from the viewpoint of noise control, the tube walls should be covered with sound-absorbing material.

### 3.1.3 Finite cylindrical pipe: acoustic resonance and sound radiation

Since most musical flue instruments are of finite length, the sound wave that propagates in the instrument bore is reflected at both open ends. As a result, the acoustic resonance occurs if the energy enough to overcome all dissipations is supplied to the bore. The acoustical condition of the bore is characterized by the input impedance or admittance in which wall boundary losses defined by  $\alpha_w$  is involved. However, the reflection is not complete, and a little of the acoustic energy confined in the bore escapes to free space. This is sound radiation, which is another source of sound dissipations in the bore.

If the resonance condition is given by  $kL = n\pi$  ( $k = \omega/c$  denotes the wave number and  $n = 1, 2, 3, \dots$ ) and the source strength of radiation at each open end is the same, we have the value of  $Q$  for sound radiation as follows [43]:

$$Q_{\text{rad}} = (n/\omega_n^2)(\pi c_0 c/R^2), \quad (37)$$

where  $\omega_n$  is the angular frequency at the  $n$ th mode resonance,  $c_0$  the sound speed in free space, and  $c$  the sound speed in the bore ( $c$  is a little smaller than  $c_0$  due to wall boundary losses [1, 43]).

Generally, the loss factor or the inverse of  $Q$  is defined as [43, 44].

$$Q^{-1} = \frac{1 \text{ time average of the power lost from the bore}}{2\pi \text{ time average of the power stored in the bore}}. \quad (38)$$

Therefore,

$$\langle \Pi_{\text{rad}} \rangle / \langle \Pi_B \rangle = 2\pi Q_{\text{rad}}^{-1}, \quad (39)$$

where  $\langle \Pi_{\text{rad}} \rangle$  denotes the time average of the power lost from the bore by sound radiation and  $\langle \Pi_{\text{B}} \rangle$  the time average of the power stored in the bore. For  $f = 300$  Hz and  $R = 25$  and  $15$  mm, we have  $Q_{\text{rad}} = 164$  and  $454$ , respectively. We can thus understand that the radiated power is very little from the evaluated values  $\langle \Pi_{\text{rad}} \rangle / \langle \Pi_{\text{B}} \rangle = 0.038$  and  $0.014$ . This implies that the first priority is clearly offered to the resonance in wind instruments. Sound radiation is only the faint leakage of the power stored in the bore. In spite of it, we can easily hear instrument tones.

$$\alpha = \alpha_{\text{w}} + \alpha_{\text{rad}} = (\omega/2c)(Q_{\text{v}}^{-1} + Q_{\text{t}}^{-1} + Q_{\text{rad}}^{-1}), \quad (40)$$

where  $\alpha_{\text{rad}}$  indicates the attenuation constant due to sound radiation. Also, the total  $Q^{-1}$  defined by Eq. (38) is equal to  $(Q_{\text{v}}^{-1} + Q_{\text{t}}^{-1} + Q_{\text{rad}}^{-1})$ . Since  $Q$  (called the quality factor) indicates the sharpness or height of the resonance, it is adequate to show  $Q$  instead of  $Q^{-1}$  for wind instruments. **Figure 11** depicts  $Q$  as a function of  $f$  for the bores of the clarinet, flute, and bass flute. We may well understand that wind instruments with cylindrical bores have appreciably high  $Q$  values over their playing ranges.

### 3.2 Acoustically induced vortices as the final dissipation agent

The above description in 3.1 on sound dissipations is correct within the scope of linear acoustics. Then, as the input energy from the player continues to increase, the output energy (viz., the sound level) from the instrument keeps increasing. However, in actual wind instruments, the saturation of the output energy necessarily occurs. In other words, sound generation is nonlinear.

An important source of the saturation in flue instruments is acoustically induced vortices (simply, acoustic vortices) at the pipe edge. These acoustic vortices work as the final dissipation agent that determines the final amplitude of the saturated sound.

#### 3.2.1 Visualization of acoustic vortices and their modeling

Jet and vortex behaviors during attack transients in organ pipe models were studied intensively using a high-speed video camera and a smoked jet in [17]. Experimental procedures are described in [17, 29]. **Figure 12(a)** and **(b)** is the visualization result which shows the exterior vortex (a) is rotating clockwise and the interior vortex (b) is rotating anticlockwise (the blowing pressure is about

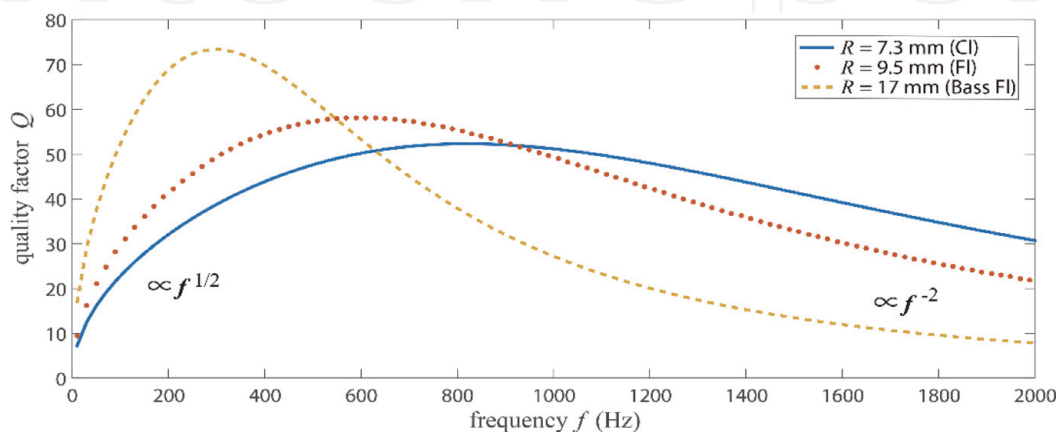


**Figure 11.** The quality factor  $Q$  as a function of  $f$  for cylindrical bore instruments. The bore radius  $R = 7.3$ ,  $9.5$ , and  $17$  mm for the clarinet, flute, and bass flute, respectively.

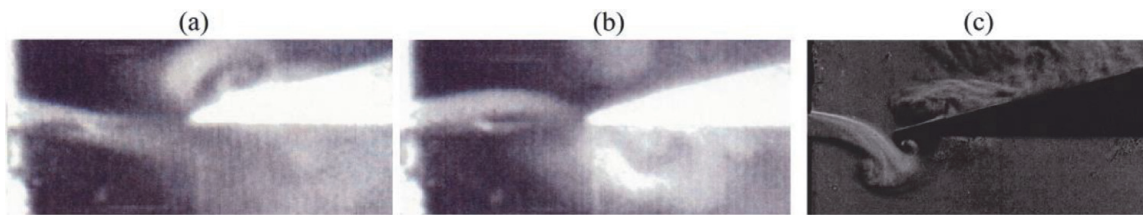


**Figure 12.**

*Visualized examples of acoustic vortices. (a) and (b): Visualized using a high-speed video camera and a smoked jet when the jet blowing pressure is 150 Pa and the sounding frequency 283 Hz [17]; (c): Visualized by means of a standard Schlieren technique when jet blowing pressure is 270 Pa and the sounding frequency 477 Hz [16]. Note that the jet-edge configuration and the buildup of the blowing pressure in frames (a) and (b) are quite different from those in frame (c). Also, frames (a) and (b) appear just before the steady state (at the “pre-steady state” in [17]), while frame (c) appears at the steady state.*

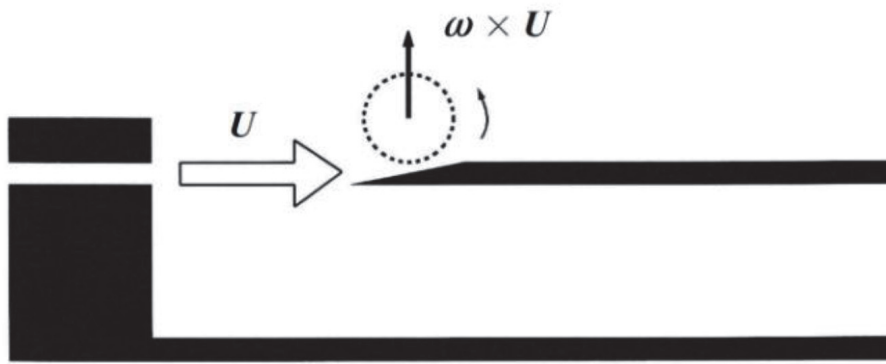
150 Pa just before the steady state and the sounding frequency 283 Hz). These vortices are making up an acoustic dipole. We can see the same rotation of the interior vortex in **Figure 12(c)**. That vortex was recognized as acoustic vortex in [16] (the steady-state blowing pressure was 270 Pa and the sounding frequency 477 Hz). Therefore, the vortices in **Figure 12(a)** and **(b)** may be regarded as acoustic vortices, too. An interior vortex is produced in **Figure 12(a)** when the jet just crosses the edge from the outside to the inside, while that in **Figure 12(c)** is produced when the jet is deflected to the inside. This difference may be due to various causes. A long flue-to-edge distance  $d$  ( $=10.2$  mm), almost null offset of the edge, a very slow buildup of the blowing pressure, and a low final blowing pressure were used in [17], while a much shorter  $d$ , a large offset, a quick buildup of the blowing pressure, and a much higher final pressure were used in [16].

These acoustic vortices shedding from the edge are considered to serve as a significant source of the sound energy dissipation in large-amplitude nonlinear oscillation [16]. According to **Figure 5** [the same organ pipe model was used in **Figures 5, 12(a)** and **(b)**], the acoustic particle velocity at the mouth is estimated as 2.3 m/s for the jet blowing velocity of 15.8 m/s (corresponding to the jet blowing pressure of 150 Pa). The acoustic velocity is thus about 15% of the flow velocity and seems to be large enough to cause nonlinear oscillations.

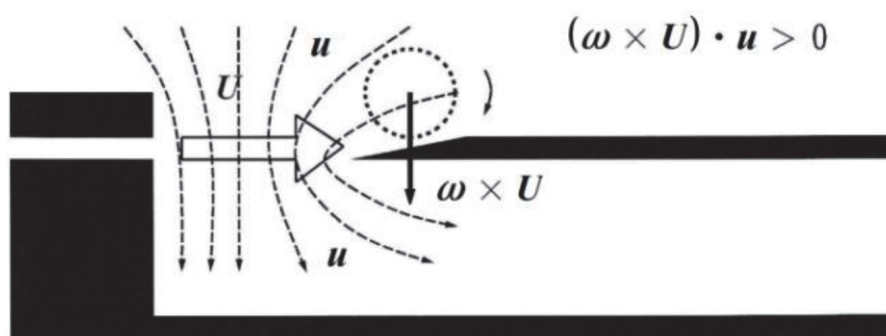
A physical modeling of the acoustic vortex generation in organ flue pipes is shown in **Figure 13** in comparison with the hydrodynamic vortex generation. A typical hydrodynamic vortex formed above the edge at the starting transient rotates anticlockwise as shown in **Figure 13(a)**. At this time the vorticity vector  $\omega$  is in the negative  $y$  direction and  $\omega \times U$  is in the positive  $z$  direction (upwards) when the jet velocity  $U$  is in the positive  $x$  direction. On the other hand, an acoustic vortex formed above the edge [see **Figure 12(a)**] rotates clockwise as shown in **Figure 13(b)**. Then,  $\omega \times U$  is in the negative  $z$  direction. Since the jet oscillates from the upward to the downward in **Figure 12(a)**, the acoustic particle velocity  $u$  takes negative maximum amplitude as known from **Figure 9(a)**. This condition is indicated by the dashed line around the mouth area in **Figure 13(b)**. As a result, the inner product  $(\omega \times U) \cdot u$  becomes positive and the absorption of sound energy by the vortex is caused according to Eq. (13). Half a period later, an acoustic vortex rotating anticlockwise is formed below the edge as shown in **Figures 12(b)** and **13(c)**, and  $\omega \times U$  as well as  $u$  is in the positive  $z$  direction. Hence,  $(\omega \times U) \cdot u$  is positive again as shown in **Figure 13(c)**, and sound energy absorption takes place at the pre-steady state or the steady state.

Although the jet deflection shown in **Figure 12(c)** is negative, the jet might be moving upward [the phase of  $\xi_e$  may be around  $12(t/T) = 1$  in **Figure 9(a)**] and then  $u$  as well as  $\omega \times U$  is possibly upward as shown in **Figure 13(c)**. Also, the effects of the pressure drive [cf. Eqs. (2) and (3)] should be considered because of

(a) Hydrodynamic vortex



(b) Acoustic vortex (exterior)



(c) Acoustic vortex (interior)

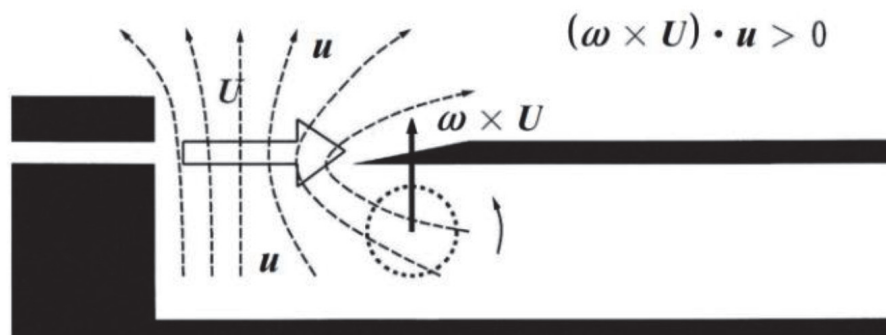


**Figure 13.** Schematic of vortex formation in organ flue pipes. (a): A hydrodynamic vortex formed at the initial phase of the starting transient; (b) and (c): An acoustic vortex formed at the pre-steady state [17].

quite high blowing pressure. The phase lag due to the pressure drive can make the acoustic velocity in the case of **Figure 12(c)** more positive as inferred from **Figure 8(a)**. Then,  $(\omega \times U) \cdot u > 0$  will be realized in better fashion.

Interestingly enough, the acoustic vortices shown in **Figure 12(a)** and **(b)** were not observed at the steady state in [17]. Instead of that, we observed a steadily deflecting jet, particularly its penetration into the pipe as captured in **Figure 13** in [17]. According to this result, we may consider that the acoustic vortex is formed to lead the finally saturated amplification of the jet stability wave by absorbing the final excess in the acoustic energy generation occurring at the pre-steady state. The acoustic vortex may be then conveyed by the jet flow into the region where the vorticity can no longer continue to interact with the acoustic field [35]. Since the completely steady state has already reached the energy balance, any more acoustic vortices seem to be not needed. Instead, the acoustic vortices will be strongly needed just before the

completely steady state or at the pre-steady state. Also, the acoustic vortex should be discussed from the common viewpoint of acoustic power dissipation and radiation of high-amplitude jet noise at duct termination [3, 15, 35, 44].

### 3.2.2 Acoustic power balance between vortex layers and acoustic vortices

Acoustic power generation by the unbalance between the upper and lower vortex layers (cf. Section 2.4) will be balanced with acoustic power dissipations by the wall boundary effects (cf. Section 3.1.2), sound radiation (cf. Section 3.1.3), and acoustic vortices in the sense of time average:

$$\langle \Pi_G(t) \rangle = \langle \Pi_\alpha(t) \rangle + \langle \Pi_D(t) \rangle, \quad (41)$$

where  $\Pi_G(t)$  is given by Eq. (14) with  $\omega = \omega_{v1}$  concerning the vortex layer,  $\Pi_\alpha(t)$  is the power lost from the bore that is given by the total attenuation constant of Eq. (40), and  $\Pi_D(t)$  is given by Eq. (13) with  $\omega = \omega_{av}$  concerning the acoustic vortex. A more exact description of  $\Pi_G(t)$  derived from the unbalance between the upper and lower vortex layers will be given in Section 4.1.

### 3.2.3 Acoustic losses due to vortex shedding at the edge

In the framework of the jet-drive model, Dequand et al. [21] assumed that the separation of the acoustic flow  $q_m(t) = (d\xi_m/dt)db$  occurs at the edge by following Verge et al. [12]. This acoustic flow separation causes a free jet [45].

Although they neglect the effects of the separation of the jet flow and their viewpoint is different from the modeling illustrated in **Figure 13**, it seems to be worth taking into consideration. The effects of vortices can be represented by a fluctuating pressure  $p_v$  across the mouth [12, 21]:

$$p_v = -(1/2)\rho(q_m/c_v db)^2 \text{sign}(q_m), \quad (42)$$

where  $c_v (= 0.6)$  is the vena contracta factor of the free jet. The time-averaged power losses due to the acoustic vortex shedding at the edge is then given as [21].

$$\langle \Pi_{\text{lost}} \rangle = \langle p_v q_m \rangle = -(1/2T)(\rho db/c_v^2) \int_0^T (d\xi_m/dt)^2 |d\xi_m/dt| dt, \quad (43)$$

where it is assumed that the dissipation occurs during the entire period  $T$ .

Therefore, the power dissipation given by Eq. (43) may be considered as an upper limit approximation, and by neglecting  $\Pi_\alpha$  in Eq. (41), it can be roughly balanced with the power generation by the jet drive given by Eq. (9) [12, 21]:

$$\langle \Pi_{\text{jet}} \rangle + \langle \Pi_{\text{lost}} \rangle \approx 0. \quad (44)$$

If the integral in the right-hand side of Eq. (43) can be replaced with a product of  $(d\xi_m/dt)_{\text{max}}^2 |d\xi_m/dt|$  and an appropriate division of  $T$  by supposing a rectangular-like waveform of  $\xi_m(t)$ , we have the following relation between the maximum acoustic velocity  $(d\xi_m/dt)_{\text{max}}$  over the mouth, the Strouhal number  $S_t = fd/U_0$ , and the aspect ratio  $d/h$  of the jet [12, 21]:

$$[(d\xi_m/dt)_{\text{max}}/U_0]^2 \sim S_t(h/d)^{3/2}. \quad (45)$$

This interesting non-dimensional relation was almost confirmed by the experiment on thin jets ( $d/h > 2$ ) for the four different flue-edge geometries (see Figure 11 in [21]). The maximum of non-dimensional amplitude  $(d\xi_m/dt)_{\max}/U_0$  reached for the edge with an angle of  $60^\circ$  is 20% higher than that obtained for the edge with an angle of  $15^\circ$ . This difference in amplitude can reflect the difference between the flute and the recorder. The recorder with a sharper edge probably brings about stronger losses due to vortex shedding at the edge.

## 4. Vortices on sound generation

In this section let us consider what the cause of the jet oscillation is for thin jets ( $d/h > 2$ ). Fletcher's displacement model of Eq. (4) [1, 31] has no definite physical basis, and Coltman's velocity model [22, 23] lacks in quantitative analysis. The present author proposed an acceleration model based on the pressure difference between the upper and lower surfaces of the jet [26]. Although this model could not involve the effects of the jet instability [20], it could successfully predict the possibility of underwater organ pipes [46]. Therefore, another acceleration model based on the vorticity generation is greatly expected [28].

### 4.1 Vortex layer along the jet visualized by PIV

A great advantage of PIV is to yield global and quantitative information on the flow-acoustic interaction. The PIV was already successfully applied to the experimental research of the edge-tone generation [6], where the complicated jet-edge interaction was investigated to accurately localize the vortex cores (dipole sources) just before the edge. Also, it was applied to measure the flow velocity and acoustic particle velocity [47]. Measurements of both quantities are required to consider sound generation based on the vortex sound theory.

#### 4.1.1 Measurement requirements

Since the vortex sound theory hypothesizes an irrotational potential flow for  $\mathbf{u}$  [18], the measurement should meet the requirement for this potential flow. However, actual acoustic cross-flow  $\mathbf{u}$  in flue instruments tends to yield a non-potential flow through any nonlinear process at large-amplitude conditions. Hence, the measurement should be carried out at low amplitudes to assure the potential flow. Moreover, the PIV cannot evaluate the contribution from the harmonics but only estimates the instantaneous flow magnitude on a plane sheet illuminated by the laser. Hence, the acoustic cross-flow should be measured based on the acoustical field with a waveform as sinusoidal as possible.

Both requirements of (1) a potential flow and (2) a sinusoidal flow for  $\mathbf{u}$  are not easily fulfilled at the same time in rigorous manner. A practical way seems to be a measurement at appropriate low amplitudes (the drive at *piano* level was better than that at *pianissimo* level [28]). Bamberger [48–50], who first introduced the PIV into the field of musical acoustics, carried out his measurement at *mezzo-forte* level by driving a flute at a very high pitch of about 1150 Hz. This sounding condition seems to satisfy the sinusoidal flow condition because a very high tone of the flute almost consists of only the fundamental. This is due to the cutoff frequency around 2 kHz of the column resonance of the modern flute [51]. However, it is uncertain whether the requirement of the irrotational potential flow on  $\mathbf{u}$  is satisfied or not. On the other hand, an organ pipe with a low-frequency resonance (at about 195 Hz)

is driven at low amplitudes to satisfy the requirement of the potential and sinusoidal flow on  $u$  simultaneously [28].

Since  $|u| \ll |U|$ , it is very difficult to measure the distribution of  $u$  over the mouth area using the PIV when the pipe is driven by the air jet. Therefore, both measurements of  $u$  and  $U$  should be separately carried out. Of course,  $U$  cannot be measured without using the jet. On the other hand,  $u$  can be measured by resonating the pipe externally, for example, by using an inverse exponential horn [28, 49]. A larger cross section of this horn is firmly fitted to the loudspeaker diaphragm, and a smaller cross section is coupled to the pipe end with a distance larger than the end correction to maintain the resonance pattern of the pressure distribution along the air column. The loudspeaker is driven by an oscillator to generate a sinusoidal wave in the pipe with the same frequency and amplitude as those when the jet drives the pipe. The organ pipe is thus driven by this loudspeaker horn system when  $u$  is measured.

Also, in order to experimentally examine the generation of the vortex sound based on Eq. (14), both measurements of  $u$  and  $U$  must be carried out at the same condition as exactly as possible. That is, these vectors must be measured at the same phase of the generating sound and at the same measurement area by using the same organ pipe. However, since  $u$  and  $U$  cannot be measured simultaneously, the jet drive and the loudspeaker horn drive must be switched as quickly as possible while maintaining the same sounding condition and the same measurement condition. The phase-locked PIV measurement on  $u$  and  $U$  (see **Figure 14**) is thus essentially important to evaluate Eq. (14). Since  $|u| \ll |U|$ ,  $u$  should be first measured using the horn drive at a given phase of the sound, and the  $U$  is measured at the same phase by quickly switching the horn drive to the jet drive.

#### 4.1.2 Measurement procedures

PIV measurement of  $u$  and  $U$  was carried out twice (Trials 1 and 2) in [28]. The fundamental frequencies of the pipe tone were 192.0 Hz and 192.1 Hz, respectively (the cutoff frequency of the horn was designed to be about 150 Hz). The averaged sound levels were 59.0 dB and 59.3 dB, respectively. When the averaged sound level was 57.8 dB (the *pianissimo* level), the third and fifth harmonics were not negligible as compared with these trials. On the other hand, when the averaged sound level was 60.2 dB, the second harmonic was only 10 dB lower than the fundamental.

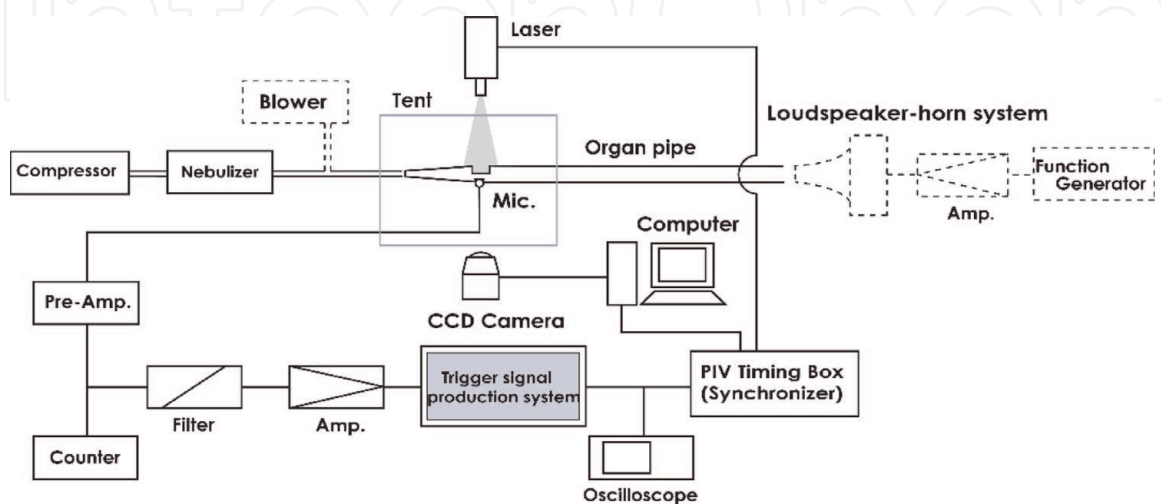


**Figure 14.** Experimental setup based on the phase-locked PIV system (the PIV itself is manufactured by Dantec dynamics). The blower and the loudspeaker horn system are alternately used for the jet drive to measure the jet velocity and for the horn drive to measure the acoustic cross-flow velocity, respectively [28].

When the level was 69.4 dB, the second harmonic showed almost the same magnitude as the fundamental. As a result, two trials above with the *piano* level excitation seem to yield good conditions satisfying the measurement requirement for  $\mathbf{u}$ . It should be noted that all these tones with their levels from 57.8 dB to 69.4 dB are produced by the same first mode resonance.

The phase lock of the PIV system is easily implemented if the external trigger signal is produced to activate the laser and the CCD camera. This is because the PIV system can set the trigger delay almost arbitrarily through the software embedded in the trigger signal production system shown in **Figure 14**. The trigger delay was set to be  $(1/12)T$  times  $n$  ( $n = 0, 1, 2, \dots, 11$ ), where  $T$  denotes the period of the pipe tone. For more details on the production of the external trigger, refer to [28]. As a result, the phase-locked measurement of  $\mathbf{u}$  and  $\mathbf{U}$  is carried out at the specific phases (Phase 0, Phase 1, Phase 2, ..., Phase 11). Note that Phase 0 is defined by the buildup of the positive trigger pulse when the trigger delay is not applied.

In the experiment a metallic organ pipe, which was made by a German organ builder, was measured [28]. Its cross-sectional structure (in  $x$ - $z$  plane) around the mouth is already shown in **Figure 1**, and its important geometry is as follows: the physical pipe length  $L = 793$  mm, the pipe inner diameter  $2R = 43.6$  mm, the flue-to-edge distance  $d = 8.8$  mm, the jet thickness  $h = 0.75$  mm, and the mouth breadth  $b = 31.9$  mm. The value of  $d/h$  is 11.7, much larger than 2. It should be noted that the edge is not very sharp like a wedge but plate-like as an extension of pipe wall, although the edge tip is 0.4 mm thick compared to the pipe wall that is 1.0 mm thick. Such an edge and flue are common in metal flue pipes as illustrated in Figure 17.6 of [1].

#### 4.1.3 Calculation of the acoustic generation formula

The PIV can derive the vorticity map from the jet velocity distribution. The vorticity  $\boldsymbol{\omega}$  ( $= \text{rot } \mathbf{U}$ ) at a field point is calculated from the 2-D velocities at four discrete points surrounding the point of interest. Therefore, the aeroacoustical source term  $\boldsymbol{\omega} \times \mathbf{U}$  and the acoustic power generation term  $(\boldsymbol{\omega} \times \mathbf{U}) \bullet \mathbf{u}$  can be calculated from the measurement of velocity fields  $\mathbf{u}$  and  $\mathbf{U}$  (see [28] on their measurement results, which are spared in this chapter).

The vorticity map given at Trial 1 is illustrated in **Figure 15(a)**. Since the 2-D velocity  $\mathbf{U}$  was measured in  $x$ - $z$  plane, the vorticity vector has only  $y$  direction component [ $\boldsymbol{\omega} = (0, \omega_y, 0)$ ]:

$$\omega_y(x, z) = \frac{\partial U_x}{\partial z}(x, z) - \frac{\partial U_z}{\partial x}(x, z). \quad (46)$$

The vorticity is formed along the upper and lower boundaries of the jet. The upper layer possesses the positive vorticity (the counterclockwise rotation of small vortices) and the lower layer the negative vorticity [cf. **Figure 10(a)**]. These layers may be called *vorticity layers* or simply *vortex layers*. At Phases 7 and 10, large-scaled positive vortices are indicated before and above the edge, but these do not seem to be important because the magnitudes of  $\mathbf{U}$  and  $\mathbf{u}$  there are very small. As a result, the effects of these vortices almost completely disappear as shown in **Figure 15(c)**. It should be correctly recognized that vortex shedding from the edge tip (cf. **Figure 6**) is never observed in **Figure 15(a)**. This implies that Howe's vortex-shedding model may not be applicable to the sound generation in organ flue pipes that are usually driven by thin jets.

The resulting aeroacoustical source term  $\boldsymbol{\omega} \times \mathbf{U}$  is displayed in **Figure 15(b)**, where the upper and lower layers of the vorticity yield the positive  $z$  and negative  $z$

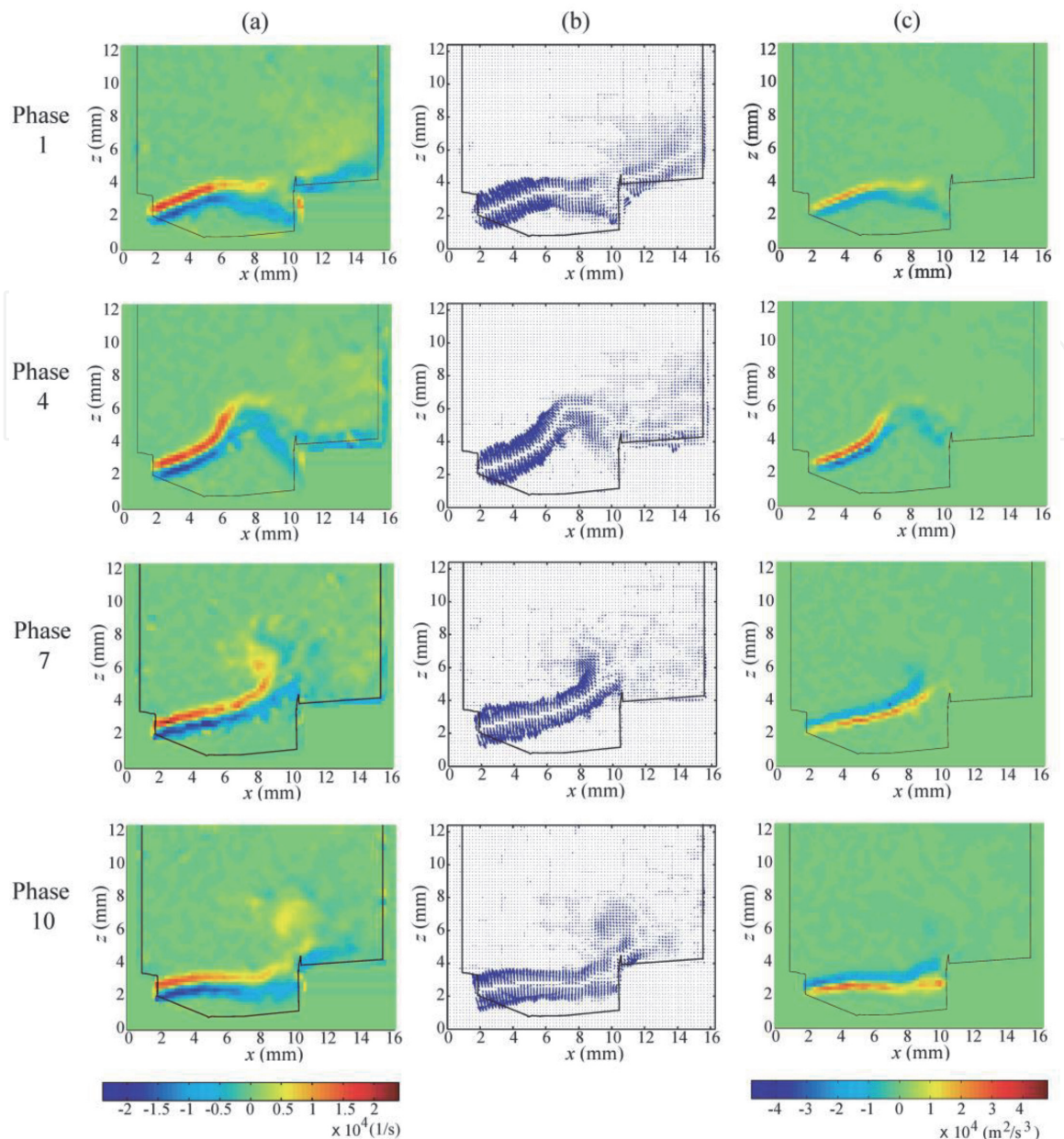


**Figure 15.** Aerodynamical quantities derived from the phase-locked PIV measurement at the organ pipe mouth: (a) vorticity  $\omega$ ; (b) aeroacoustical source term (acceleration)  $\omega \times U$ ; (c) acoustic generation term  $(\omega \times U) \cdot \mathbf{u}$ . The positions of the flue exit and the edge tip correspond to  $(x, z) = (2.0 \text{ mm}, 2.2 \text{ mm})$  and  $(x, z) = (10.5 \text{ mm}, 3.8 \text{ mm})$ , respectively [28].

components of  $\omega \times U$ , respectively. The maximum magnitude of  $\omega \times U$ , which is about  $2 \times 10^5 \text{ (m/s}^2\text{)}$ , can be observed near the flue. The opposing vectors of  $\omega \times U$  along both layers seem to almost cancel each other as depicted in **Figure 10(b)**. However, since  $\omega \times U$  has a very large acceleration, an imperfect cancellation (or a slight unbalance) between  $\omega \times U$  vectors along both layers yields a significant effect in acoustical events.

#### 4.1.4 Generation of the acoustic power from the vortical field

Acoustic generation term  $(\omega \times U) \cdot \mathbf{u}$  defined by Eq. (14) is shown in **Figure 15(c)**. Since  $\mathbf{u}$  indicates the outflow at Phases 1 and 4, and inflow at Phases 7 and 10,  $(\omega \times U) \cdot \mathbf{u}$  takes the opposite sign along the vortex layer between these phases. This sign inversion occurs near Phases 0 and 6 [28]. The maximum magnitude of  $(\omega \times U) \cdot \mathbf{u}$  appears near 1–2 millimeters downstream from the flue at Phases 3 and 8 as about

$4.2 \times 10^4 \text{ (m}^2/\text{s}^3)$ . The jet crosses the edge from the inside at Phase 3 and from the outside at Phase 8 as inferred from **Figure 15(c)**. Although the magnitude of  $(\boldsymbol{\omega} \times \mathbf{U}) \cdot \mathbf{u}$  is relatively small near the edge, it should be noted that  $(\boldsymbol{\omega} \times \mathbf{U}) \cdot \mathbf{u}$  originally has very large values in acoustical sense.

Since the volume integral defined by Eq. (14) is not easily executed, the acoustic power generation from the vortex layer is estimated from the following surface integral by assuming the 2-D property (see Figure 11 in [28]) of  $\mathbf{u}$  and  $\mathbf{U}$ :

$$\partial \Pi_G(t) / \partial y \approx - \iint \rho (\boldsymbol{\omega} \times \mathbf{U}) \cdot \mathbf{u} dx dz. \quad (47)$$

This surface integral, which may be called the *instantaneous 2-D vortex sound power*, is carried out at each phase, and the result is represented in **Figure 16(a)** and **(b)** concerning Trials 1 and 2, respectively. The integral area is restricted to  $1 \leq x \leq 13 \text{ mm}$  and  $1 \leq z \leq 9 \text{ mm}$  to reduce the calculation error caused from the area irrelevant to the acoustic generation term. Also, another scale of the ordinate is added to the right side of **Figure 16** in order to give a rough estimate of the magnitude of  $\Pi_G(t)$ . Since the mouth breadth  $b$  of our organ pipe is 31.9 mm,  $\Pi_G(t)$  is estimated as  $[\partial \Pi_G(t) / \partial y] \times 0.030 \text{ (m)}$  by assuming almost perfect 2-D property of  $\mathbf{u}$  and  $\mathbf{U}$ .

Significant double-peak structure of  $\Pi_G$  is clearly demonstrated in **Figure 16(a)**. A larger peak is indicated at Phases 2, 3, and 4 when the jet crosses the edge from the inside and moves to the outside (cf. **Figure 15**). On the other hand, a smaller peak is shown at Phases 10 and 11 when the jet enters deeply into the pipe. It should be noted that the jet crosses the edge from the outside at Phase 8 and almost null vortex sound power is generated at Phase 8. Hence, this smaller peak occurs in a little phase delay from the impingement of the jet against the edge. The temporal average of  $\Pi_G$  estimated from the 2-D vortex sound power in **Figure 16(a)** will take a definitely positive value. Therefore, it may be recognized that the acoustic power is generated from the jet vortex layers. Although **Figure 16(b)** shows the characteristics similar to those of **Figure 16(a)**, the value at Phase 3 seems to be too large and erroneous because of the instant when the jet impinges against the edge [28].

#### 4.1.5 Dominant area for the acoustic power generation and receptivity problem

The maps of the vorticity and aeroacoustical source term definitely indicate much larger magnitudes at the flue side as shown in **Figure 15(a)** and **(b)**, respectively. On the other hand, the acoustic flow velocity takes much larger magnitudes

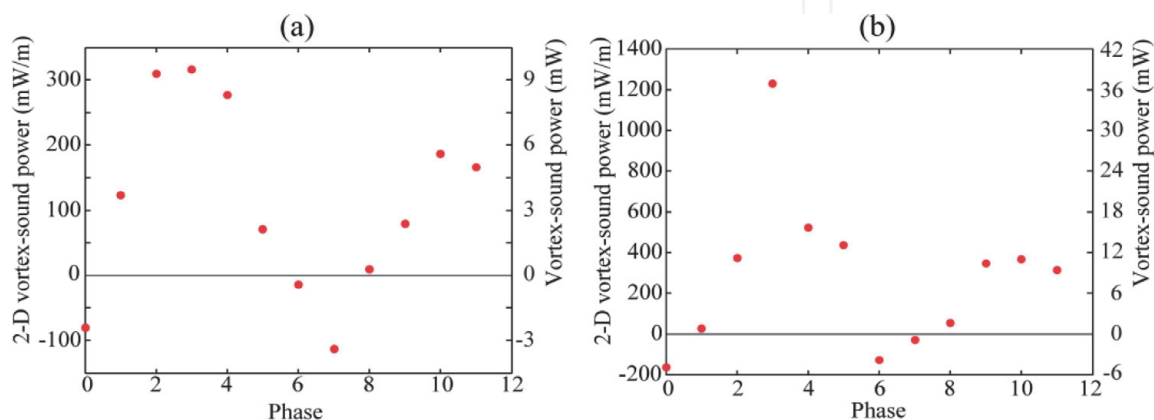


**Figure 16.**

The 2-D vortex sound power (left ordinate) and vortex sound power (right ordinate) as a function of the phase: (a) trial 1 and (b) trial 2 [28].

at the edge side (see Figures 5(a) and 7 in [28]). It should be then discussed which side is more dominant for the acoustic power generation.

The area for the surface integral of Eq. (47) is now set to be  $2 \leq x \leq 11$  mm and  $1 \leq z \leq 6$  mm. Then, this area is divided into two at  $x = 7, 8,$  and  $9$  mm. Hence, we have six sub-areas with the same  $z$  extent. The calculation result is demonstrated in Figure 12 of [28]. A very sharp contrast is displayed between area 5 ( $2 \leq x \leq 9$  mm) and area 6 ( $9 \leq x \leq 11$  mm): Area 5 yields larger negative values of  $\partial \Pi_G(t)/\partial y$  at Phases 3, 4, and 5; area 6 yields much larger positive values of  $\partial \Pi_G(t)/\partial y$  at the same phases. Hence, it may be concluded that such a small area as area 6 (very close to the edge) is most responsible for the acoustic power generation whose instantaneous contributions are given from Phases 2 to 5.

Also, the phase relation between the jet displacement, the acoustic velocity, and the acoustic pressure at the edge can be considered based on the PIV measurement results. The result is the same as **Figure 9(a)** (see Figure 13 in [28]). The dominant sound generation in our PIV experiment occurs with a phase lag of about  $60 - 90^\circ$  from the jet impingement against the edge [28]. This seems to verify that our experiment satisfies the requirements for the volume-flow model.

Coltman [52] discussed the activating force for the jet wavy motion. This is the most difficult problem in the flue instrument acoustics and is defined as the problem of the *receptivity* (the generation of jet oscillation by acoustic flow perturbations at the flue exit) [10]. Our present study based on the PIV measurement demonstrated that the aeroacoustic source term  $\omega \times U$  (having the dimension of the acceleration) associated with the vortex-layer formation along the jet could activate the jet oscillation in an organ pipe. More precisely, an incomplete cancelation (or a net unbalance) of  $\omega \times U$  between both sides of the jet can activate (oscillate) the jet.

Since this  $\omega \times U$  can also activate the jet motion in the edge-tone generation [3–6, 18], the vortex-layer formation may be regarded as the fluid-dynamical mechanism common to the edge-tone generation and the pipe-tone generation. This fluid-dynamical model, which is a leading candidate to solve the receptivity problem, may be referred to as the *acceleration unbalance model* [28]. In the acoustical framework, this model can lead the volume-flow drive in an organ pipe driven by a thin jet with relatively low blowing pressures. Helmholtz might have envisaged such a physical picture as mentioned in Section 2.4.

## 4.2 Vortices from the jet visualized by direct numerical simulations

Sound generation in flue instruments is the revelation of the fluid *compressibility* in *low* Mach number state. This is a contradicting phenomenon in fluid-dynamical sense. Because of this, direct numerical simulations based on the Navier–Stokes equation could not achieve satisfactory outcomes [2]. However, in the 2010s we had many outstanding results from various viewpoints [53–55]. They are mentioning the roles of vortices, but do not have resolution enough to discuss the almost invisible (to our naked eyes) microstructure in the jet and its boundaries, particularly vortices in jet vortex layers, which seem to be a key point to solve the receptivity problem in the near future.

For the sake of page limitation, the description here is restricted to an essential point given by Eq. (24), which manifests the importance of the acoustic velocity  $u_f(t)$  at the flue exit. By reformulating Fletcher's displacement model given by Eq. (4), Onogi et al. [56] proposed another formula that decomposed the jet oscillation into hydrodynamic and acoustic displacements, which were simulated on the basis of the 3-D compressible Navier–Stokes equations. They supposed the non-zero initial amplitude at the flue exit and the variable oscillation center with the flow direction for the jet displacement, although Coltman [52] strongly denied Fletcher's

displacement model. Their simulation results (see Figures 7, 9, and 10 and Table IV in [56]) seem to confirm the non-zero amplitude at the flue exit, and the acoustic feedback effects on the jet wave may be given at its starting point.

## 5. Conclusions

Vortices on sound generation are clearly revealed in edge tones (with thin jets, without any resonators) and cavity tones (with thick, almost semi-infinite, jets, with cavity resonators). Although visible, relatively large vortices are seen in flue instruments driven by thick jets, these are in rare cases. Usually flue instruments are driven by thin jets [(jet length  $d$ /jet thickness  $h$ )  $> 2$ ]. Any visible, discrete vortices do not appear at the flue exit and at the pipe edge in those cases. Instead, vortex layers are formed along the jet upper and lower boundaries, and the acceleration unbalance between them drives the jet as a whole in flue instruments.

The jet-wave drive (or the volume-flow drive) and the vortex-layer drive by thin jets assure sound generation in good manner when the jet enters into the pipe at the instant when the acoustic pressure is maximum. In the discrete-vortex drive by thick jets, the acoustic cross-flow (particle velocity) takes positive and negative values during the passage of the lower and upper vortices from the flue exit to the pipe edge, respectively. These vortex configurations can create sound power during the former and latter halves of an oscillation period.

On the other hand, acoustically induced vortices universally appear as the final dissipation agent. Their role in acoustic energy balance near the saturated state in flue instruments should be reconfirmed in more detail to exactly judge whether the acoustic vortex is generated just at the saturated state or just before the saturated state (at the pre-saturated state).

The receptivity problem is a key point to elucidate the sounding mechanism in flue instruments from the fluid-dynamical viewpoint. The initial amplitudes of acoustic quantities at the flue exit are regarded as the starting point for the acoustic feedback effects upon the jet wave. The vortex-layer model above will then be expected to solve this problem with the aid of direct aeroacoustical simulations.

## Acknowledgements

The present author expresses his appreciation to three European scientists: Dr. Judit Angster of Fraunhofer-Institute für Bauphysik, in Stuttgart, for her long-term support to carry out the PIV measurement; Prof. Avraham Hirschberg of Technische Universiteit Eindhoven for his kind offer of the picture used as **Figure 12(c)** and helpful comments to the author's journal papers from the aeroacoustical viewpoint; and Prof. Andreas Bamberger of Freiburg University for his effective comments and suggestions on the PIV. Also, the author thanks Keita Arimoto and Takayasu Ebihara of Yamaha Corporation, in Hamamatsu, Japan, for their sincere support and appropriate comments to the manuscript.

IntechOpen

IntechOpen

### **Author details**

Shigeru Yoshikawa  
Kyushu University, Dazaifu, Japan

\*Address all correspondence to: [shig@lib.bbiq.jp](mailto:shig@lib.bbiq.jp)

### **IntechOpen**

---

© 2020 The Author(s). Licensee IntechOpen. This chapter is distributed under the terms of the Creative Commons Attribution License (<http://creativecommons.org/licenses/by/3.0>), which permits unrestricted use, distribution, and reproduction in any medium, provided the original work is properly cited. 

## References

- [1] Fletcher NH, Rossing TD. The Physics of Musical Instruments. 2nd ed. New York: Springer-Verlag; 1998. p. 690
- [2] Yoshikawa S. Fluid-dynamical models of musical wind instruments. In: Yoshikawa S, Wada H, editors. Aeroacoustics of Sound Sources. Tokyo: Corona Publishing Co. Ltd; 2007. pp. 207-252. (in Japanese)
- [3] Howe MS. Acoustics of Fluid-Structure Interactions. New York: Cambridge University Press; 1998. p. 570
- [4] Powel A. On the edge-tone. Journal of the Acoustical Society of America. 1961;**33**:395-409
- [5] Holger KD, Wilson TA, Beavers GS. Fluid mechanics of the edge-tone. Journal of the Acoustical Society of America. 1977;**62**:1116-1128
- [6] Lin J-C, Rockwell D. Oscillations of a turbulent jet incident upon an edge. Journal of Fluids and Structures. 2001; **15**:791-826
- [7] Rockwell D, Naudascher E. Review—self-sustaining oscillations of flow past cavities. Journal of Fluids and Engineering, Transactions of ASME. 1978;**100**:152-165
- [8] Elder SA. Self-excited depth-mode resonance for a wall-mounted cavity in turbulent flows. Journal of the Acoustical Society of America. 1978;**63**:877-890
- [9] Meissner M. Aerodynamically excited acoustic oscillations in cavity resonator exposed to an air jet. Acta Acustica united with Acustica. 2002;**88**: 170-180
- [10] Fabre B, Hirschberg A. Physical modeling of flue instruments: A review of lumped models. Acta Acustica united with Acustica. 2000;**86**:599-610
- [11] Elder SA. The mechanism of sound production in organ pipes and cavity resonators. Journal of the Acoustical Society of Japan (E). 1992;**13**:11-23
- [12] Verge MP, Fabre B, Hirschberg A, Wijnands APJ. Sound production in a recorder-like instrument. Part 1: Dimensionless amplitude of the internal acoustic field. Journal of the Acoustical Society of America. 1997;**101**:2914-2924
- [13] Segoufin C, Fabre B, Verge MP, Hirschberg A, Wijnands APJ. Experimental study of the influence of the mouth geometry on sound production in a recorder-like instrument: Windway length and chamfers. Acta Acustica united with Acustica. 2000;**86**:649-661
- [14] Hirschberg A. Aeroacoustics of wind instruments. In: Hirschberg A, Kergomard J, Weinrich A, editors. Mechanics of Musical Instruments. Wien: Springer-Verlag; 1995. pp. 291-369
- [15] Bechert DW. Sound absorption caused by vorticity shedding, demonstrated with a jet flow. Journal of Sound and Vibration. 1980;**70**:389-405
- [16] Fabre B, Hirschberg A, Wijnands APJ. Vortex shedding in steady oscillation of a flue organ pipe. Acta Acustica united with Acustica. 1996;**82**:863-877
- [17] Yoshikawa S. A pictorial analysis of jet and vortex behaviours during attack transients in organ pipe models. Acta Acustica united with Acustica. 2000;**86**: 623-633
- [18] How MS. Contributions to the theory of aerodynamic sound, with application to excess jet noise and the theory of the flute. Journal of Fluid Mechanics. 1975;**71**:625-673

- [19] Rayleigh L. *The Theory of Sound*. New York: Macmillan; 1894. Reprinted by Dover; 1945. pp. 376-414
- [20] Cremer L, Ising H. Die selbsterregten Schwingungen von Orgelpfeifen. *Acoustica*. 1967/1968;**19**: 143-153
- [21] Dequand S, Willems JFF, Leroux M, Vullings R, van Weert M, Thieulot C, et al. Simplified models of flue instruments: Influence of mouth geometry on the sound source. *Journal of the Acoustical Society of America*. 2003;**113**:1724-1735
- [22] Coltman JW. Sounding mechanism of the flute and organ pipe. *Journal of the Acoustical Society of America*. 1968; **44**:983-992
- [23] Coltman JW. Jet drive mechanism in edge tones and organ pipes. *Journal of the Acoustical Society of America*. 1976; **60**:725-733
- [24] Elder SA. On the mechanism of sound production in organ pipes. *Journal of the Acoustical Society of America*. 1973;**54**:1554-1564
- [25] Fletcher NH. Jet drive mechanism in organ pipes. *Journal of the Acoustical Society of America*. 1976;**60**:481-483
- [26] Yoshikawa S, Saneyoshi J. Feedback excitation mechanism in organ pipes. *Journal of the Acoustical Society of Japan (E)*. 1980;**1**:175-191
- [27] Verge MP, Causse R, Fabre B, Hirschberg A, Wijnands APJ, van Steenberg A. Jet oscillations and jet drive in recorder-like instruments. *Journal of the Acoustical Society of America*. 1994;**80**:403-419
- [28] Yoshikawa S, Tashiro H, Sakamoto Y. Experimental examination of vortex-sound generation in an organ pipe: A proposal of jet vortex-layer formation model. *Journal of Sound and Vibration*. 2012;**331**:2558-2577
- [29] Yoshikawa S. Jet-wave amplification in organ pipes. *Journal of the Acoustical Society of America*. 1998;**103**:2706-2717
- [30] Helmholtz HLF. *On the Sensations of Tone*. Berlin: Springer; 1863. Reprinted by Dover; 1954. pp. 88-94 (translated by A. J. Ellis in English)
- [31] Fletcher NH. Sound production by organ flue pipes. *Journal of the Acoustical Society of America*. 1976;**60**: 926-936
- [32] Mattingly GE, Criminale WO Jr. Disturbance characteristics in a plane jet. *Physics of Fluids*. 1971;**14**:2258-2264
- [33] Michalke A. On spatially growing disturbances in an inviscid shear layer. *Journal of Fluid Mechanics*. 1965;**23**: 521-544
- [34] Drazin PG, Howard LH. Hydrodynamic stability of parallel flow of in-viscid fluid. *Advances in Applied Mechanics*. 1966;**9**:1-89
- [35] Howe MS. The dissipation of sound at an edge. *Journal of Sound and Vibration*. 1980;**70**:407-411
- [36] Brown GB. The vortex motion causing edge tones. *Proceedings of the Physical Society of London*. 1937;**49**: 493-507
- [37] Brown GB. The mechanism of edge-tone production. *Proceedings of the Physical Society of London*. 1937;**49**: 508-521
- [38] Auvray R, Ernoult A, Fabre B, Lagrée P-Y. Time-domain simulation of flute-like instruments. Comparison of jet-drive and discrete-vortex models. *Journal of the Acoustical Society of America*. 2014;**136**:389-400

- [39] Tsuchida J, Fujisawa T, Yagawa G. Direct numerical simulation of aerodynamic sounds by a compressible CFD scheme with node-by-node finite elements. *Computational Methods on Applied Mechanical Engineering*. 2006; **195**:1896-1910
- [40] de la Cuadra P. The sound of oscillating air jet. Physics, modeling and simulation in flute-like instruments. Ph. D. thesis. University of Stanford; 2005
- [41] Auvray R, Lagrée P-Y, Fabre B. Regime change and oscillation thresholds in recorder-like instruments. *Journal of the Acoustical Society of America*. 2012; **131**:1574-1585
- [42] Meyer E, Neumann E-G. Attenuation of sound. In: *Physical and Applied Acoustics*. New York: Academic Press; 1972. pp. 95-115
- [43] Yoshikawa S. Energy dissipations in underwater and aerial organ pipes. *Journal of the Acoustical Society of Japan (E)*. 1984; **5**:181-192
- [44] Salikuddin M, Ahuja KK. Acoustic power dissipation on radiation through duct termination: Experiments. *Journal of Sound and Vibration*. 1983; **91**:479-502
- [45] Ingard KU, Ising H. Acoustic nonlinearity of an orifice. *Journal of the Acoustical Society of America*. 1967; **42**: 6-17
- [46] Yoshikawa S. Underwater organ pipes. *Journal of the Acoustical Society of Japan (E)*. 1984; **5**:211-221
- [47] Hann DB, Greated CA. The measurement of flow velocity and acoustical particle velocity using particle-image velocimetry. *Measurement Science and Technology*. 1997; **8**:1517-1522
- [48] Bamberger A. Investigations and recent results on flutes with PIV. In: *Proceedings of the Forum Acusticum*. Sevilla, Spain; 2002. MUS -04-003-IP
- [49] Bamberger A. Vortex sound of flutes observed with particle image velocimetry. In: *Proceedings of 18th International Congress on Acoustics*. Kyoto, Japan; 2004. pp. 1417-1420
- [50] Bamberger A. Vortex sound in flutes using flow determination with Endo- PIV. In: *Proceedings of the Forum Acusticum*. Budapest, Hungary; 2005. pp. 665-670
- [51] Wolfe J, Smith J. Cutoff frequencies and cross fingering in baroque, classical, and modern flutes. *Journal of the Acoustical Society of America*. 2003; **114**:2263-2272
- [52] Coltman JW. Jet behavior in the flute. *Journal of the Acoustical Society of America*. 1992; **92**:74-83
- [53] Miyamoto M, Ito Y, Iwasaki T, Akamura T, Takahashi K, Tamaki T, et al. Numerical study on acoustic oscillation of 2D and 3D flue organ pipe like instruments with compressible LES. *Acta Acustica united with Acustica*. 2013; **99**:154-171
- [54] Giordano N. Simulation studies of the recorder in three dimensions. *Journal of the Acoustical Society of America*. 2014; **135**:906-916
- [55] Yokoyama H, Miki A, Onitsuka H, Iida A. Direct numerical simulation of fluid-acoustic interactions in a recorder with tone holes. *Journal of the Acoustical Society of America*. 2015; **138**: 858-873
- [56] Onogi K, Yokoyama H, Iida A. Analysis of jet oscillations with acoustic radiation in the recorder by direct aeroacoustic simulations. *Journal of the Acoustical Society of America*. 2019; **146**:1427-1437